Received: 5 October 2017 | Revised: 13 February 2018 | Accepted: 21 February 2018

DOI: 10.1002/cne.24438

RESEARCH ARTICLE

WILEY JCN RESEARCH IN SYSTEMS NEUROSCIENCE THE JOURNAL OF COMPARATIVE NEUROLOGY

Partitioning of the primate intraparietal cortex based on connectivity pattern and immunohistochemistry for Cat-301 and SMI-32

Otavio S. C. Mariani[1,2] | Bruss Lima[1] | Juliana G. M. Soares[1] | Andrei Mayer[1] | João G. Franca[1] | Ricardo Gattass[1]

[1]Institute of Biophysics Carlos Chagas Filho, Federal University of Rio de Janeiro, Rio de Janeiro, RJ 21949-902, Brazil

[2]School of Physical Therapy, University of São Carlos, São Paulo, Brazil

Correspondence
Ricardo Gattass, Instituto de Biofísica Carlos Chagas Filho, Bloco G, CCS, UFRJ, Ilha do Fundão, Rio de Janeiro, RJ, 21941-902, Brazil.
Email: rgattass@gmail.com

Funding information
FAPERJ (PRONEX), Grant/Award Number: E-26/210.917/2016, E-26/110.905/2013; FINEP, Grant/Award Number: PEC20150; CNPq, Grant/Award Number: 471.166/2013-8; Serrapilheira Institute, Grant Number: Serra-1709-17523

Abstract

We propose a partitioning of the primate intraparietal sulcus (IPS) using immunoarchitectural and connectivity criteria. We studied the immunoarchitecture of the IPS areas in the capuchin monkey using Cat-301 and SMI-32 immunohistochemistry. In addition, we investigated the IPS projections to areas V4, TEO, PO, and MT using retrograde tracer injections in nine hemispheres of seven animals. The pattern and distribution of Cat-301 and SMI-32 immunostaining revealed multiple areas in the IPS, in the adjoining PO cleft and in the annectant gyrus, with differential staining patterns found for areas V3d, DM, V3A, DI, PO, POd, CIP-1, CIP-2, VIPa, VIPp, LIPva, LIPvp, LIPda, LIPdp, PIPv, PIPd, MIPv, MIPd, AIPda, AIPdp, and AIPv. Areas V4, TEO, PO, MT, which belong to different cortical streams of visual information processing, receive projections from at least twenty different areas within the IPS and adjoining regions. In six animals, we analyzed the distribution of retrogradely labeled cells in tangential sections of flat-mount IPS preparations. The lateral bank of the IPS projects to regions belonging both to the ventral (V4 and TEO) and dorsal (PO and MT) streams. The region on the floor of the IPS (i.e., VIP) projects predominantly to dorsal stream areas. Finally, the medial bank of the IPS (i.e., MIP) projects solely to the dorsalmedial stream (PO). Therefore, our data suggest that ventral and dorsal streams remain segregated within the IPS, and that its projections to the dorsal stream can be further segregated based on those targeting the dorsolateral versus the dorsomedial subdivisions.

KEYWORDS

Intraparietal cortex, Cat-301, SMI-32, V4, TEO, PO and MT connections

1 | INTRODUCTION

The intraparietal sulcus (IPS), located on the lateral surface of the parietal lobe, contains several subregions that are architectonically and functionally distinct (Pandya & Seltzer, 1982; Luppino, Ben Hamed, Gamberini, Matelli, & Galletti, 2005; Gregoriou, Borra, Matelli, & Luppino, 2006; Rizzolatti, Luppino, & Matelli, 1998). These areas have been intensively investigated using both single-unit electrophysiology

Abbreviations: AIP, anterior intraparietal area; amt, anterior middle temporal sulcus; ar, arcuate sulcus; ca, calcarine fissure; ce, central sulcus; ci, cingulate sulcus; CIP-1, caudal intraparietal area 1; CIP-2, caudal intraparietal area 2; co, collateral sulcus; DI, dorsointermediate area; DM, dorsomedial area; dp, dorsal pre-lunate area; ec, external calcarine sulcus; FST, visual area at the fundus of the superior temporal sulcus; io, inferior occipital sulcus; ip or ips, intraparietal sulcus; la, lateral sulcus; LIPd, dorsal portion of lateral intraparietal area; LIPv, ventral portion of lateral intraparietal area; lu, lunate sulcus; MIP, medial intraparietal area; MST, medial superior temporal area; MT, visual area MT; MTp, peripheral portion of MT; orb, orbital sulcus; ot, occipitotemporal sulcus; p, principal sulcus; PCi, parieto-cingulate area; PIP, posterior intraparietal area; pmt, posterior middle temporal sulcus; PO, parieto-occipital area; pom, medial parieto-occipital sulcus; rh, rhinal sulcus; sp, subparietal sulcus; st, superior temporal sulcus; TEa, anterior portion of area TE; TEm, medial portion of area TE; TEO, posterior inferior temporal cortex; TEp, posterior portion of area TE; TH, cytoarchitectonic area TH; V1, primary visual cortex; V2, visual area 2; V3A, visual complex V3, part A; V3d, dorsal portion of visual area 3; V3v, ventral portion of visual area 3; V4, visual area 4; V4t, V4 transition zone; VIP, ventral intraparietal area; VTF, visual portion of parahippocampal TF.

J_ID: Customer A_ID: CNE24438 Cadmus Art: CNE24438 Ed. Ref. No.: CASA-JCN-17-0236.R1 Date: 4-April-18 Stage: Page: 2

in primates (Colby & Goldberg, 1999; Andersen, 1989), and functional neuroimaging in humans (Culham & Kanwisher, 2001). Areas of the IPS are believed to be involved in perceptual-motor coordination (e.g., directing eye movements and reaching) and visual attention, which allow for visually guided pointing, grasping, and object manipulation in goal-directed tasks.

Currently, at least five regions of the IPS have been shown to be associated with specific behaviors: lateral intraparietal area (LIP) and ventral intraparietal area (VIP) are involved in visual attention and saccadic eye movements (Andersen, 1989; Colby & Goldberg, 1999); VIP and medial intraparietal area (MIP) are involved in visual control of reaching and pointing (Colby & Duhamel, 1991; Duhamel, Colby, & Goldberg, 1992; Colby, Duhamel, & Goldberg, 1993); anterior intraparietal area (AIP) is related to visual control of grasping and manipulating hand movements (Sakata, Taira, Murata, & Mine, 1995; Rizzolatti et al., 1998; Murata, Gallese, Luppino, Kaseda, & Sakata, 2000); while caudal intraparietal (CIP) areas are involved in depth perception from stereopsis (Sakata, 2003; Tsutsui, Jiang, Sakata, & Taira, 2003). However, previous studies have not offered precise anatomical criteria capable of delimiting the IPS areas being investigated. As a result, the current subdivisions of the IPS are based on coarse topographical features.

Over the past 30 years, we have been studying the capuchin monkey brain using multiple approaches, which include electrophysiology, anatomy, connectivity pattern, cytoarchitecture, chemoarchitecture, myeloarchitecture, and behavior. The *Sapajus apella* (formally, *Cebus apella*) or capuchin monkey is a New Old diurnal monkey with brain size and sulcal pattern similar to the Old World monkey genus *Macaca*. The aim of the present work is to describe the location, extent, and borders of the areas located within the IPS of the capuchin monkey using immunoarchitectural and connectivity criteria. The partitioning of cortical areas in the adjoining PO (parietooccipital) cleft and annectant gyrus are also reported here. As immunoarchitectural makers capable of revealing structural features of IPS neurons, we used monoclonal antibodies that bind to chondroitin sulfate proteoglycans (Cat-301) or to nonphosphorylated epitopes in neurofilament proteins (SMI-32). To study the connectivity pattern of the IPS, we injected retrograde tracers in areas V4, TEO, PO, and MT (middle temporal area), and studied the layer-specific projections originating from the different IPS regions. Connectivity data were used to corroborate and refine the IPS partitioning obtained through Cat-301 and SMI-32 immunohistochemistry.

We were able to delimit the following areas within the IPS: posterior intraparietal (PIP), MIP (with its ventral and dorsal subdivisions), CIP-1, CIP-2, VIP, AIP (proper, and its dorso-posterior and dorso-anterior subdivisions) and LIP (with its ventral, dorsal, anterior, and posterior subdivisions). We were also able to define areas PO, POd (dorsal portion of PO), V3A, DM (dorsomedial) and DI (dorsointermediate) in the adjoining PO cleft and annectant gyrus using Cat-301 immunohistochemistry.

Studies of V2, V4, TEO, TE, and PO connectivity in the macaque have revealed extensive projections between area PO and the areas of IPS, while V2 and V4 have been shown to be weaklier interconnected with the IPS (Colby, Gattass, Olson, & Gross, 1988; Webster, Bachevalier, & Ungerleider, 1994; Gattass, Sousa, Mishkin, & Ungerleider, 1997; Ungerleider, Galkin, Desimone, & Gattass, 2008). Here we show that areas V4 and TEO show a complimentary pattern of connectivity with the IPS as compared to areas PO and MT, suggesting that the ventral and dorsal streams of visual information processing remain segregated within this region. Finally, the differential connectivity between IPS and areas PO and MT corroborate the notion that the dorsal stream can be further sub-divided into dorsolateral and dorsomedial components (Gattass et al., 1990; Nascimento-Silva, Gattass, Fiorani, & Sousa, 2003).

2 | MATERIALS AND METHODS

All experimental protocols were conducted following the NIH guidelines for animal research and were approved by the committee for animal care and use of the Instituto de Biofísica Carlos Chagas Filho, UFRJ. Seven adult *Sapajus apella* monkeys ranging in weight from 2.8 to 4.0 kg were used in this study. Five of these animals were also used in other unrelated anatomical studies.

Anesthesia was induced with an intramuscular injection of 30 mg/kg of ketamine hydrochloride (Ketalar; Parke Davis, Rio de Janeiro, Brazil). In addition, animals also received 0.15 mg/kg of atropine sulfate (Atropina; Roche, São Paulo, Brazil) to reduce salivation and other secretions, and 0.8 mg/kg of benzodiazepine (Valium, Roche) to induce sedation. Anesthesia was maintained with an intravenous infusion of sodium thiopental (Tiopental, Cristália, São Paulo, SP, Brazil—10 mg/kg/h) in 5% of glucose or with regularly repeated intramuscular injections of a 1:5 mixture of 6% ketamine hydrochloride and 2% dihydroxylazine hydrochloride (Rompun, Bayer, Rio de Janeiro, RJ, Brazil). The levels of expired CO_2, rectal temperature, and heart rate were continuously monitored throughout the experiment and maintained within physiological ranges. A craniotomy was made over the intended injection sites under sterile conditions, and the dura mater was sectioned to expose the cortical surface. Injections were made under visual guidance or electrophysiological mapping guidance. Following the tracer injections, the wound was closed in anatomical layers, and the animals received prophylactic intramuscular injections of penicillin G (Benzetacil - 300.000 UI – EUROFARMA, São Paulo, SP, Brazil).

2.1 | Tracer injections

Pressure injections into the cortex were made using a 1 μL Hamilton syringe fitted with a beveled 27-gauge needle, which was guided into the appropriate site with the aid of an operating microscope. Sulcus and gyral landmarks were used to identify the location of areas V4 and TEO (Zeki, 1978; Ungerleider & Desimone, 1986b; Gattass, Sousa, & Gross, 1988). As a reference to guide the injections, we used the superficial blood vessel located over the superior temporal gyrus (this vessel travels through the inferior occipital and the superior temporal sulci). Volumes ranging from 0.2 to 1 μL of retrograde tracers were injected into the cortical surface of the target areas. In seven cases, 1–13 injections (0.15–0.3 μL each at each site) of aqueous solutions containing 2% Fast Blue (FB, Polysciences, Inc.), 5% Diamidino Yellow (DY, Polysciences, Inc.), 4% Fluoruby (FR, Molecular Probes) or 10% Texas Red

J_ID: Customer A_ID: CNE24438 Cadmus Art: CNE24438 Ed. Ref. No.: CASA-JCN-17-0236.R1 Date: 4-April-18 Stage: Page: 3

(TR, Sigma-Aldrich) were placed in a given cortical area. For cases involving both a 10% solution of wheat germ agglutinin conjugated to horseradish peroxidase (HRP-WGA, Sigma, St. Louis, MO) and other tracer injections, the non-HRP tracer or tracers were first injected into V4, then given an interval of 4–6 days before HRP was injected into another site. To minimize leakage of the tracer up the electrode track, the syringe was left in place for 30 min after the injection and then withdrawn into the guide tube, which was then removed from the brain. In the remaining three animals, after the desired injection site was located using electrophysiological guidance, a guide tube was advanced through the dura and placed about 300 μm above the intended injection site. The microelectrode was then advanced through the guide tube and the visuotopic representation of the injection site confirmed by receptive field mapping. The electrode was then withdrawn from the guide tube and replaced by a 1-μL Hamilton syringe. Injections of FB, DY, FR, and TR were made into one or both hemi- T1 spheres in each animal for a total of seven hemispheres (see Table 1). For the V4, TEO, and MT injections, we inferred the eccentricity of the injections based on the location of the feedback projections from V2, using the visuotopic map described by Rosa, Souza, and Gattass (1988).

2.2 | Perfusion and anatomical processing

After of 7–21 days of survival, the animals received lethal intraveneous doses of sodium pentobarbital (50 mg/kg) and were transcardially perfused using saline and fixation solutions. The cortex of five animals underwent a flattening procedure of the occipital lobe, while the remaining brains were cut in the coronal or oblique section planes. To obtain flattened cortical preparations for the first five animals, they were initially perfused with 0.9% saline followed by 0.1 M phosphate buffer at pH 7.4. Next, the brains were removed from the skull, reduced into a block that included areas V1, V2, V4, and MT and then flattened. The IPS was dissected for flattening, separately. The tissue block was carefully unfolded, interposed and gently pressed between glass slides, and submersed in a fixation solution. This preparation was fixed with a solution of 4% paraformaldehyde in 0.1 M phosphate buffer during 12 hr and stored overnight in phosphate buffer/glycerol (10%). Frozen 60 mm-thick sections were obtained in a plane tangential to the pia mater.

The animals designated for Cat-301 (Case 6) and SMI-32 (Case 7) immunohistochemistry were perfused initially with 0.9% saline, followed by a sequence of the solutions including 4% paraformaldehyde in phosphate-buffered saline (PBS), 4% paraformaldehyde in PBS with 2.5% glycerol, PBS with 5% glycerol, and then PBS with 10% glycerol. After removal from the skull, the brain was immersed in the latter solution overnight. The next day, it was frozen and cut into 40 μm-thick sections using a cryostat. The angle of section was oblique relative to the coronal plane for the Cat-301 immunohistochemistry (see brain F1 illustration in Figure 1). In this way, we were able to include areas of the IPS and of the annectant gyrus within the same slice. We used parasagittal sections for SMI-32 immunohistochemistry. Alternate sections were stained for cell bodies using cresyl violet, or for fibers using the Gallyas' method (Gallyas, 1979).

2.3 | Immunohistochemical reactions

2.3.1 | Cat-301

For the immunoarchitectural study of IPS areas, sections were stained using Cat-301 or SMI-32 monoclonal antibodies. Cat-301 is a monoclonal antibody that recognizes a 680-kD chondroitin sulfate proteoglycan similar to aggrecan, which is a high-molecular-weight chondroitin sulfate proteoglycan found in cartilage. In the central nervous system, Cat-301 immunoreactivity is localized to the extrasynaptic surface of neurons. It has been hypothesized by Hockfield and co-workers (1990) that a Cat-301-binding proteoglycan is a molecular marker indicating that a neuron has acquired mature neuronal properties. The Cat-301 antibody recognizes epitopes belonging to magnocellular-related structures, preferentially in area V1 and extrastriate areas of humans, apes, Old World and New World monkeys (DeYoe, Hockfield, Garren, & Van Essen, 1990). Mize and Hockfield (1989) have shown that, in the visual system, Cat-301 selectively labels Y-like cells in several structures, including portions of the lateral geniculate nucleus complex and visual cortex.

For immunohistochemistry reaction, sections were incubated overnight with Cat-301 antibody (1:500, Chemicon, Millipore Corporation. Cat# MAB5284, RRID: AB_2219944) in a solution containing 0.05% bovine albumin and 0.3% triton X-100 in 0.01 M PBS at a pH of 7.4. Sections were then incubated for an additional hour in biotinylated anti-rabbit secondary antibody and then processed by the avidin–biotin method. For both reactions, immunoreactivity was revealed with 0.05% 3,3′-diaminobenzidine (DAB) and 0.1% nickel ammonium sulfate. Sections were then mounted on bi-gelatinized slides, dehydrated in increasing alcohol concentrations (75–90–100–100%, 1 min each), defatted in xylene (2 × 3 min) and coverslipped with DPX.

Control sections were prepared by omitting the primary antibody in the incubation solution (McKay & Hockfield, 1982; Hockfield, Mckay, Hendry, & Jones, 1983). These sections showed no specific staining.

2.3.2 | SMI-32

The SMI-32 monoclonal antibody recognizes a nonphosphorylated epitope on the 168 kDa and 200 kDa subunits of neurofilament proteins, thus labeling the cell body and dendrites of a subset of pyramidal neurons. SMI-32-immunoreactive neurons exhibit consistent differences in the intensity of their labeling that correlated well with cell size. The size, density, and laminar distribution of SMI-32-immunoreactive neurons differed substantially across neocortical areas, and has been shown to be a very useful histological tool for cortical partitioning in primates (Campbell & Morrison, 1989; Hof & Morrison, 1995; Lewis & Van Essen, 2000; Soares, Rosado De Castro, Fiorani, Nascimento-Silva, & Gattass, 2008; Cruz-Rizzolo, De Lima, Ervolino, de Oliveira, & Casatti, 2011; Mayer et al., 2016). Similar to macaques (Campbell & Morrison, 1989; Hof & Morrison, 1995; Lewis & Van Essen, 2000), SMI-32 immunohistochemistry in the capuchin monkey reveals a heterogeneous labeling pattern in the cortex (Soares et al., 2008; Cruz-Rizzolo et al., 2011; Mayer et al., 2016), where two bands with varying levels of SMI-32 immunoreactivity are

J_ID: Customer A_ID: **CNE24438** Cadmus Art: **CNE24438** Ed. Ref. No.: **CASA-JCN-17-0236.R1** Date: **4-April-18** Stage: Page: **4**

TABLE 1 Relative strength of the IPS projections to areas V4, TEO, PO, and MT

Cases and Intraparietal projections	Case 1				Case 2				Case 3				Case 4			
	V4		TEO		V4		TEO		V4		TEO		V4		TEO	
	superf.	deep	superf.	deep	superf.	deep	superf.	deep	superf.	deep	superf.	deep	superf.	deep	superf.	deep
V3A	+	+	+	++	+	+	+	++	+	+	++	+	+	+	+	++
DI	+	++	+	++	++	+++	+	++	+++	++++	+++	++	+++	++++	+++	++
DM	++++	+++	++	+	++	+	++	+	+++	++	++	++	++	+	++	+
7a			+	+			+	+		+	+	+		+	+	+
CIP-1	+	++	+	++	++	+++	+	++	+	+++	+++	++	++	+++	+++	++
CIP-2			+++	++	+	+	+				+++	+			+++	+
LIPvp	+++	+++			+++	+++	+	+	+++	++	+++	++	+++	++	+++	++
LIPva	+	++	+	++	++	+++	+++	+	++	+++	+++	+	++	+++	+++	++
LIPdp			++	++			+	+		+	++	+			++	+
LIPda	+	+	++++	+++	++	+++	++++	+++	++	+++	++++	++++	++	+++	++++	++++
AIP v					++	+										
AIPdp																
AIPda																
VIPp																
VIPa																
PIP	++	++	+	+	++	++	+	+	+++	++	+		+++	++	+	
MIP																
PO		+								+	+		+	+	+	
5d	+				+											

	Case 5								Case 6							
	V4		TEO		PO		MT		V4		TEO		PO		MT	
	superf.	deep	superf.	deep	superf.	deep	superf.	deep	superf.	deep	superf.	deep	superf.	deep	superf.	deep
V3A	+	+		+	+			+	+	+		+	+			+
DI	++	+++		+	+		+	++	++	+++		+	+		+	++
DM	+++	++	++	+	+	+	+	++	++	++	++	+	+	+	+	+
7a					++	+++		+		+			++	+++		+
CIP-1	+	++	+++	++	+++	+++	+	+	+	+++	+++	++	+++	+++		+
CIP-2			+++		+++	+					+++		+++	+		
LIPvp	+++	+++			++	++	+	++	++	++			++	++	+	++
LIPva	++	+++	+++	+	++	++	+	+	+++	+++	+++	+	+++	++	+	+
LIPdp		+			+	++		+					+	++	+	+
LIPda	++	+++	++++	+++	+	++	+	+	++	+++	++++	+++	+	++	+	+
AIP v	++	+	+		++				++		+		++			
AIPdp	++	+				++	+	++	++	+				++	+	++
AIPda							+	+							+	+
VIPp	+	+			++	+++		++	++	+			++	+++		++
VIPa					++	+++		++					+	+++		++
PIP	+++	+	+		++++	+++			++	+	+		+++++	+++		
MIP		+			+++	+++							+++++	+++		
PO	+		+		n/a	n/a		+			+		n/a	n/a	+	++
5d	+					+	+	+	+						+	+

Data is split relative to the laminar profile of the projections and the six cases (nine hemispheres) studied. Label density in each area was independently estimated for each individual tracer and assigned to six (i.e., 0–5) different intensity levels (represented by the + symbol).

J_ID: Customer A_ID: CNE24438 Cadmus Art: CNE24438 Ed. Ref. No.: CASA-JCN-17-0236.R1 Date: 4-April-18 Stage: Page: 5

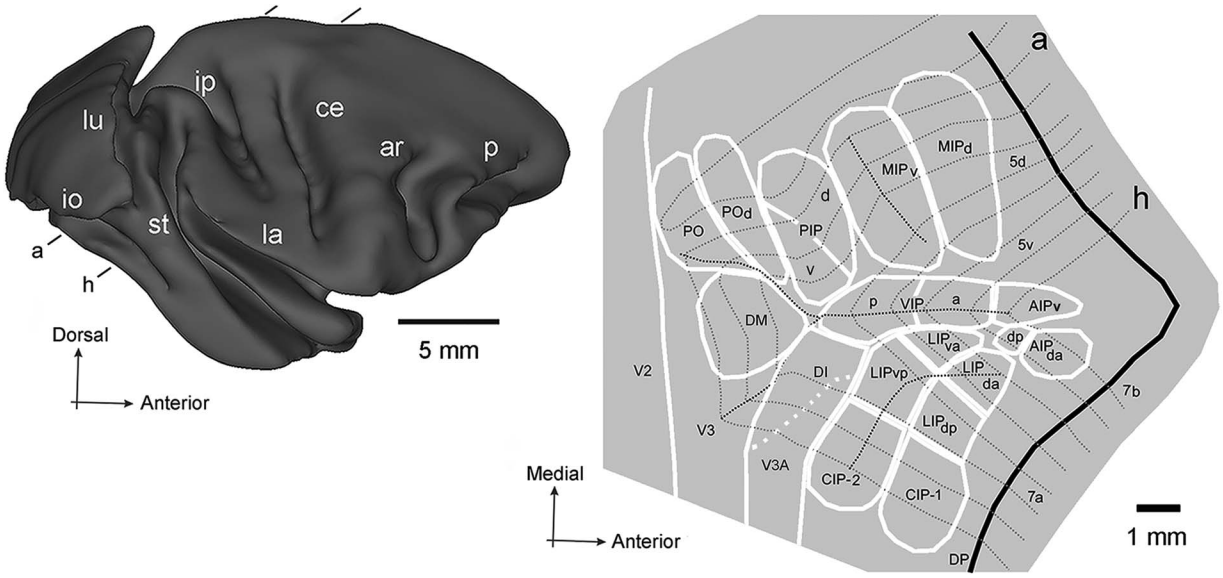

FIGURE 1 Subdivisions of the IPS based on Cat-301 immunohistochemistry. Part I: A three-dimension image of the right hemisphere of the capuchin brain (cortical sulci open for illustration purposes) is depicted on the left. A flattened representation of the IPS is shown on the right, with areal borders depicted in white. The black continuous line represents the edges of the IPS. Short line segments (left panel) and black dashed lines (right panel) indicate the level of the oblique coronal sections illustrated in Parts II and III. Sections (a–h) are equally spaced from one another. Part II: Oblique coronal sections of the right hemisphere of the capuchin monkey brain encompassing a large extent of the IPS, the adjoining PO cleft and the annectant gyrus. Histological sections were immunoreacted for Cat-301 and ordered from posterior (a) to anterior (c), as indicated in Part I (left panel). A schematic representation of a full brain section at the level shown in (a) is depicted on the top right. Boundaries between areas are indicated by black arrows. Part III: The subsequent histological sections (d–h) anterior to those shown in Part II. Abbreviations: lu, lunate sulcus; io, inferior occipital sulcus; ip or ips, intraparietal sulcus; st or sts, superior temporal sulcus; la, lateral sulcus; ce, central sulcus; ar, arcuate sulcus; p, principal sulcus; ca, calcarine fissure; ls, lateral sulcus; cis, cingulate sulcus

usually observed over layers III and V. These two bands are composed of small to large pyramidal neurons, including their proximal processes and fragments of apical dendrites.

In order to reveal SMI 32 immunoreactivity, free-floating sections were initially washed three times in phosphate buffer-saline (PBS) 0.1 M for 10 min, and subsequently incubated with 2% bovine serum albumin (BSA) in a solution of 0.3% Triton X-100 in PBS (PBS-Tx), for 1 hr, at room temperature. After three rinses in PBS, sections were gently shaken overnight at room temperature in a solution of mouse monoclonal IgG 1 SMI-32 antibody (1:5,000, Covance Research Products Inc. Cat# SMI-32R-500, RRID:AB_509998) in a 2% BSA solution diluted in 0.3% PBS-Tx. Sections were then washed three times in PBS, incubated in biotinylated secondary horse anti-mouse antibody (1:200, Vector Laboratories) for 2 hr, at room temperature, washed again (3 × 10 min in PBS) and incubated for 1 hr using the Vectastain ABC System (1:500 Vector Laboratories) at room temperature.

2.4 | Tangential cutting

In our tangential sectioning of the flattened cortex (50 μm thick sections), the depth of the section indicated the cortical layer we were at. Cutting from the pial surface to the white matter, the first section corresponds to the top of layer I, while the last section (usually section number 37) corresponds to the bottom of layer VI. For oblique sections, we used reconstruction techniques in order to study the distribution of labeled cells across the different cortical layers.

2.5 | Data analysis

Photomicrographs of cortical sections were obtained using a Zeiss Axioplan-2 microscope equipped with a color digital camera (1600 × 1200, 3/4" chip, 36 bit, MBF) and a motorized stage (Mac5000 LUDL) controlled by Neurolucida software (MBF Biosciences, Inc; RRID:nif-0000–10294) running on a Dell workstation. Images from entire histological slides were produced with the aid of the Virtual Tissue 2D module. With this module, a series of optical images containing adjacent parts of a same section were systematically acquired using a 5× (Zeiss Plan-Neofluoar) objective, and then unified into a single image of the whole section. Before image acquisition, color balance was adjusted to reduce background noise. Additional brightness and contrast corrections were performed in the acquired image as a whole. Borders between areas were established only after agreement between at least two independent investigators. The criteria used to differentiate cortical areas, and thereby establish areal borders in histological sections stained with Cat-301 or SMI-32 antibodies included size, density and laminar distribution of the immunoreactive cell bodies. Additional criteria included the extension and thickness of reactive

J_ID: Customer A_ID: CNE24438 Cadmus Art: CNE24438 Ed. Ref. No.: CASA-JCN-17-0236.R1 Date: 4-April-18 Stage: Page: 6

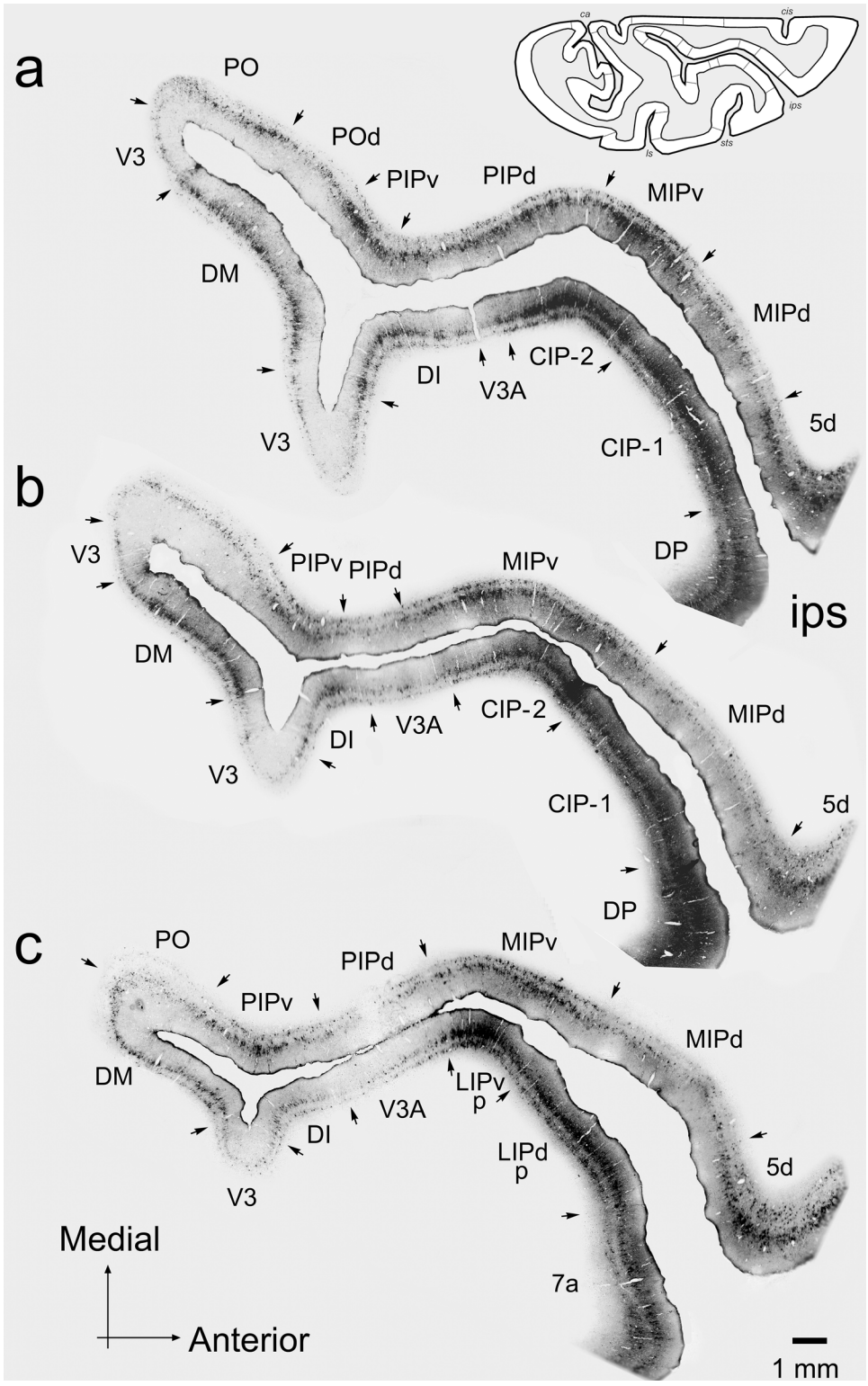

FIGURE 1 Continued

apical dendrites and the intensity of neuropil reactivity across the different cortical layers. Differences in laminar thickness between cortical regions were also used as criteria to define IPS areas. In order to transform the immunoarchitectural Cat-301 data, such as those shown in Figure 1 (Parts II and III), into a "map" of the IPS, we first unfolded the relevant portions of IPS by building a three-dimensional model and then flattening it. Sections through IPS were traced at 10× magnification and a wire bent to conform to layer IV of each section. The wires were then attached with scaled cross pieces to form a three-dimensional model of the banks of

J_ID: Customer A_ID: CNE24438 Cadmus Art: CNE24438 Ed. Ref. No.: CASA-JCN-17-0236.R1 Date: 4-April-18 Stage: Page: 7

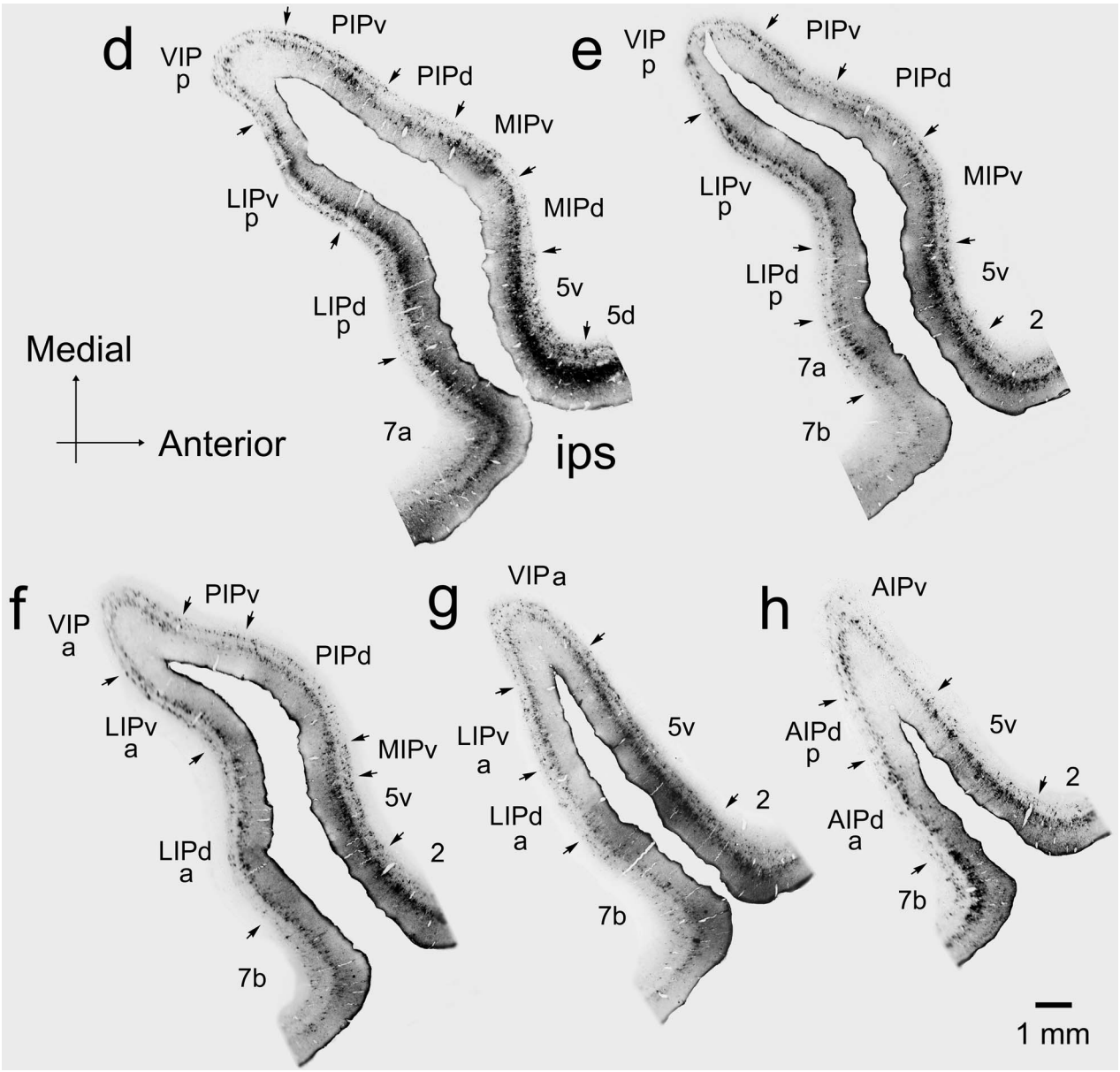

FIGURE 1 Continued

the sulcus. The model was then unfolded (flattened) by hand, to form a two-dimensional surface. A flattened model is illustrated in Figure 1 (Part I, right panel).

For Case 7, a two-dimensional reconstruction of the neocortex was done based on the contours of layer IV using sections placed 1.6 mm apart, as described by Van Essen and Maunsell (1980). The architectonic boundaries were subsequently transferred onto the flattened maps. For Case 6, we performed a three-dimensional reconstruction of the cortical surface using the CARET software (Van Essen et al., 2001) in order to illustrate the spatial organization of the intraparietal areas of the capuchin monkey. For SMI-32, contours of histological sections containing the limits of cortical layer IV were drawn using the Neurolucida Neuron Tracing Software (MBF Bioscience), and the borders between different cortical areas were identified.

3 | RESULTS

In this study, we define the location, extension, and borders of the cortical areas located in the primate using immunoarchitectural and connectivity data. As immunoarchitectural markers we used the Cat-301 and SMI-32 monoclonal antibodies that target, respectively, chondroitin sulfate proteoglycans and neurofilament H proteins. Additionally, we injected retrograde tracers in areas V4, TEO, PO, and MT in order to study the layer-specific pattern of IPS projections to these four visual areas. The immunoarchitectural markers were able to provide a first clear partitioning of IPS areas (Figures 1–4). Connectivity data, which we analyzed independently, confirmed and often refined the areal borders defined immunoarchitecturally. For Cat-301 immunohistochemistry and retrograde tracer experiments we analyzed, in addition to the IPS, areas partially or entirely belonging to the adjoining PO cleft and

J_ID: Customer A_ID: **CNE24438** Cadmus Art: **CNE24438** Ed. Ref. No.: **CASA-JCN-17-0236.R1** Date: **4-April-18** Stage: Page: **8**

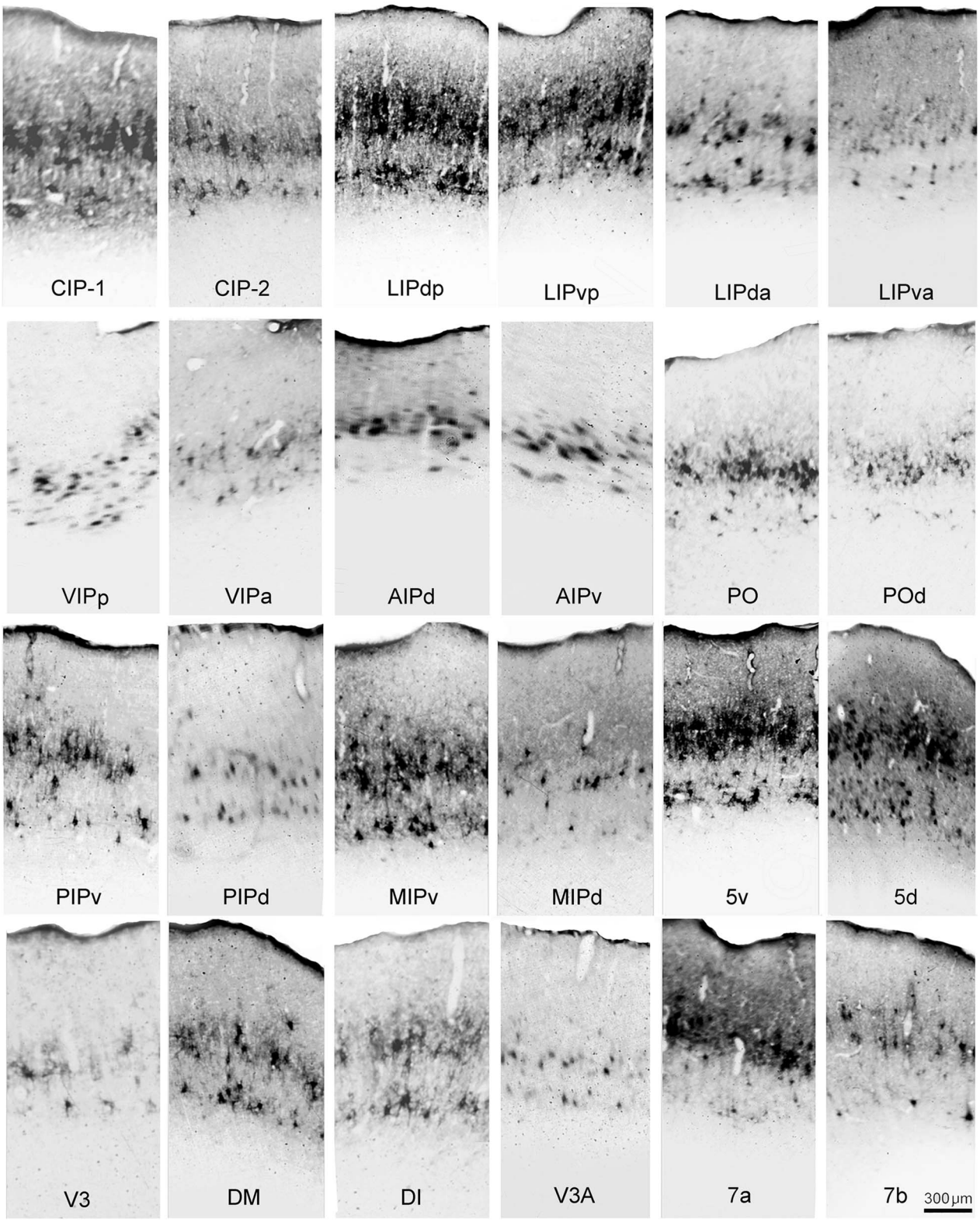

FIGURE 2 High power photomicrographs of the IPS areas revealed by Cat-301 immunohistochemistry shown in Figure 1. See Results for a detailed description of the immunoarchitectural organization of each area. Cell bodies in layers III and V were the predominant structures revealed by Cat-301 immunostaining (note the two stripes, more or less evident, in each one of the panels). Additionally, the neuropil of layers II/III could also be differentially labeled. For example, note the strong neuropil labeling of area LIP, but not of area PO

J_ID: Customer A_ID: CNE24438 Cadmus Art: CNE24438 Ed. Ref. No.: CASA-JCN-17-0236.R1 Date: 4-April-18 Stage: Page: 9

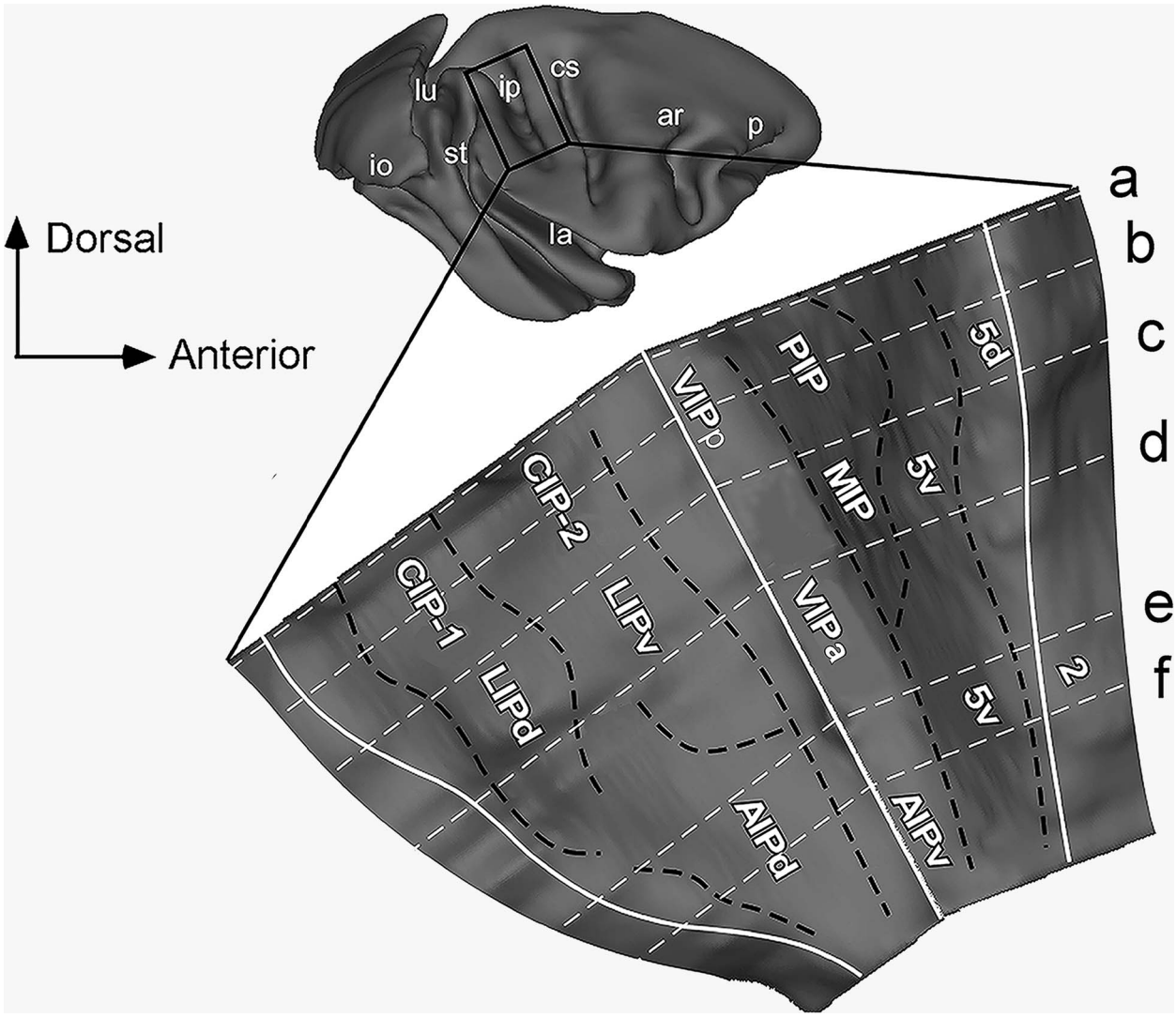

FIGURE 3 Subdivisions of the IPS based on SMI-32 immunohistochemistry. Part I: The top panel shows a three-dimension image of the right hemisphere of the capuchin brain (cortical sulci open for illustration purposes). The IPS is depicted below in a flattened representation at the level of cortical layer IV. Black dashed lines represent borders between cortical areas. White continuous lines indicate the fundus and the edges of the IPS. White dashed lines indicate the levels of the parasagittal sections. Part II: (a–f) Parasagittal sections of the right hemisphere of the capuchin monkey brain encompassing a large extent of the IPS. Histological sections were immunoreacted for SMI-32 and ordered from medial (a) to lateral (f), as indicated in the flattened representation in Part I. Boundaries between areas are indicated by black arrows. Abbreviations as in Figure 1

annectant gyrus, namely PO, POd, V3A, DI, V3d, and DM. We were thereby also able to establish their borders and connectivity patterns with areas V4, TEO, PO, and MT. In particular, we were able to ascertain the presence of areas DM and DI in the capuchin monkey. This wide scope analysis allowed us to refine the areal borders we have proposed in previous work (Colby et al., 1988; Gattass et al., 1997; Ungerleider et al., 2008), re-designate POm as the area medial to PO and POd, and propose a new designation to the area medial to MIP, which we named the parieto-cingulate area (PCi).

3.1 | Areal subdivisions revealed by Cat-301 and SMI-32 immunohistochemistry

Immunohistrochemistry using the Cat-301 and SMI-32 antibodies allows for a consistent partitioning of the IPS. The immunoarchitectural organization revealed by Cat-301 immunohistochemistry is shown in Figure 1 (Parts I–III). In addition, Figure 2 exhibits enlarged images of the IPS areas shown in Figure 1. The corresponding results for SMI-32 immunohistochemistry are shown in Figures 3 and 4. Both immune reactions label mainly medium and large-size pyramidal neurons in layers III and V, some nonpyramidal cells in layers III and V, and scattered small-size neurons in layer VI. However, they show differences in the density of labeled cells and neuropil across distinct areas. SMI-32 immunoreactivity allowed for the segregation of about 12 areas (CIP-1, CIP-2, LIPd, LIPv, VIPp, VIPa, MIP, PIP AIPd, AIPv, area 5v, and area 5d). More medial areas, such as PO and POd could not be identified due to the angle of our histological sectioning for SMI-32. Cat-301 immunoreactivity, on the other hand, revealed more than 20 cortical areas in the IPS and in the adjoining PO cleft and annectant gyrus. It turned out that each area revealed by SMI-32 immunolabeling could be

J_ID: Customer A_ID: CNE24438 Cadmus Art: CNE24438 Ed. Ref. No.: CASA-JCN-17-0236.R1 Date: 4-April-18 Stage: Page: 10

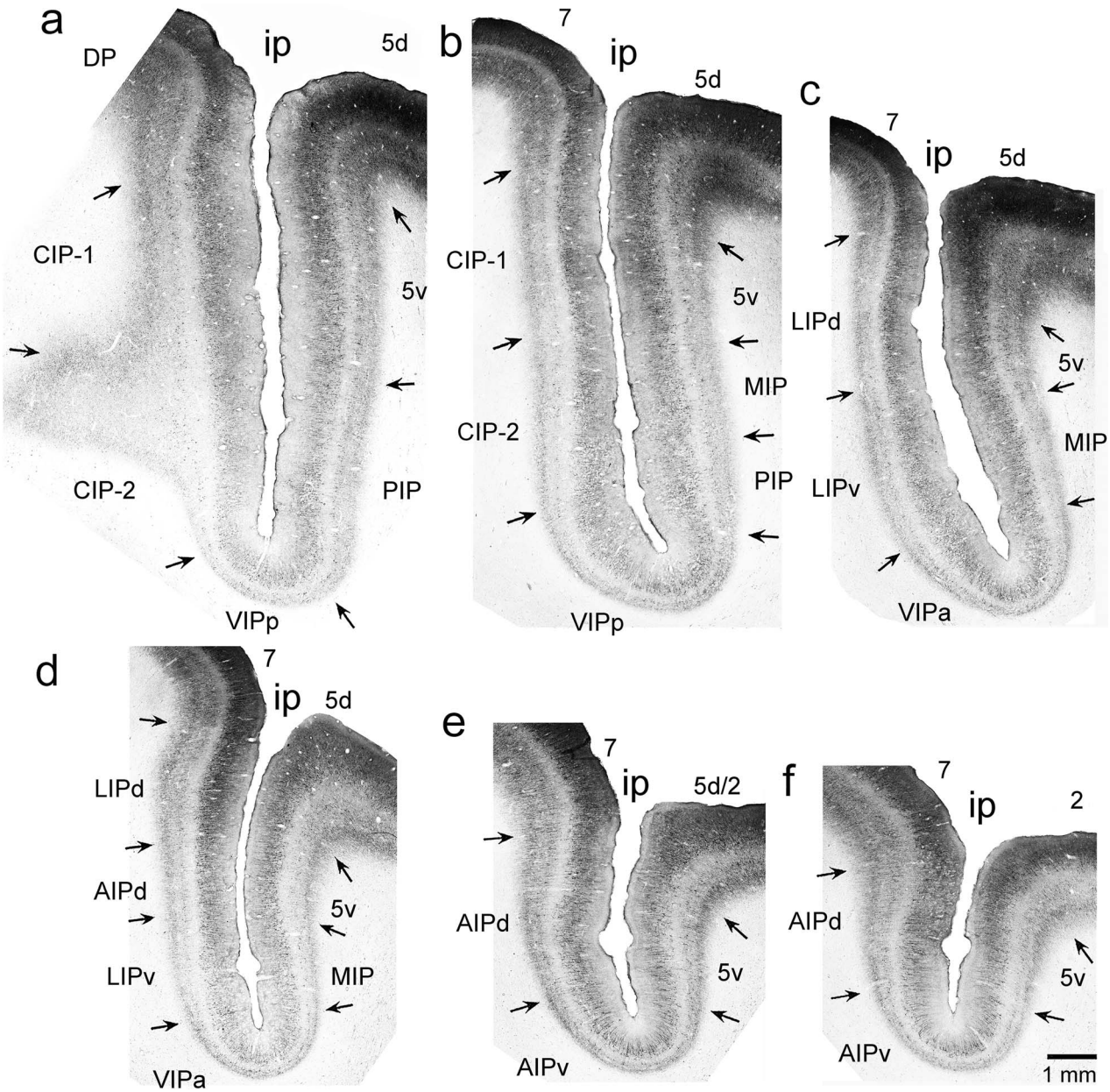

FIGURE 3 Continued

further subdivided into two or more areas by Cat-301 immunolabeling, as described in detail below.

3.2 | CIP-1

Area CIP-1 is located in the lateral (posterior) bank of the IPS, at this caudal portion. It is limited dorsally by DP, ventrally by CIP-2, anteriorly by LIPdp, and posteriorly by V3A. It is characterized by intense immunoreactivity for SMI-32 in the supra- and infragranular layers, with a large number of strongly stained pyramidal cells located mainly in layer III, and a lower number of smaller nonpyramidal and pyramidal cells in layers V and VI (refer to Figures 3 and 4 for the IPS partitioning based on SMI-32 immunohistochemistry). Area CIP-1 presents a continuous but diffuse Cat-301 labeling in layer III, and a coarse labeling in layer V (refer to Figures 1 and 2 for the IPS partitioning based on Cat-301 immunohistochemistry). The upper layers have a faint light labeling of the neuropil. We found a medium to strong labeling in layer III, characterized by strongly packed pyramidal neurons, and medium strength labeling in the lower layers, characterized by stellate and pyramidal cells.

3.3 | CIP-2

Area CIP-2 is located in the lateral bank of the IPS, ventrally to CIP-1. It is limited anteriorly by LIPvp, and posteriorly by V3A. CIP-1 differs from CIP-2 by presenting a smaller number of SMI-32 and Cat-301 labeled neurons in layer III, and a less densely stained neuropil in layers V and VI.

J_ID: Customer A_ID: CNE24438 Cadmus Art: CNE24438 Ed. Ref. No.: CASA-JCN-17-0236.R1 Date: 4-April-18 Stage: Page: 11

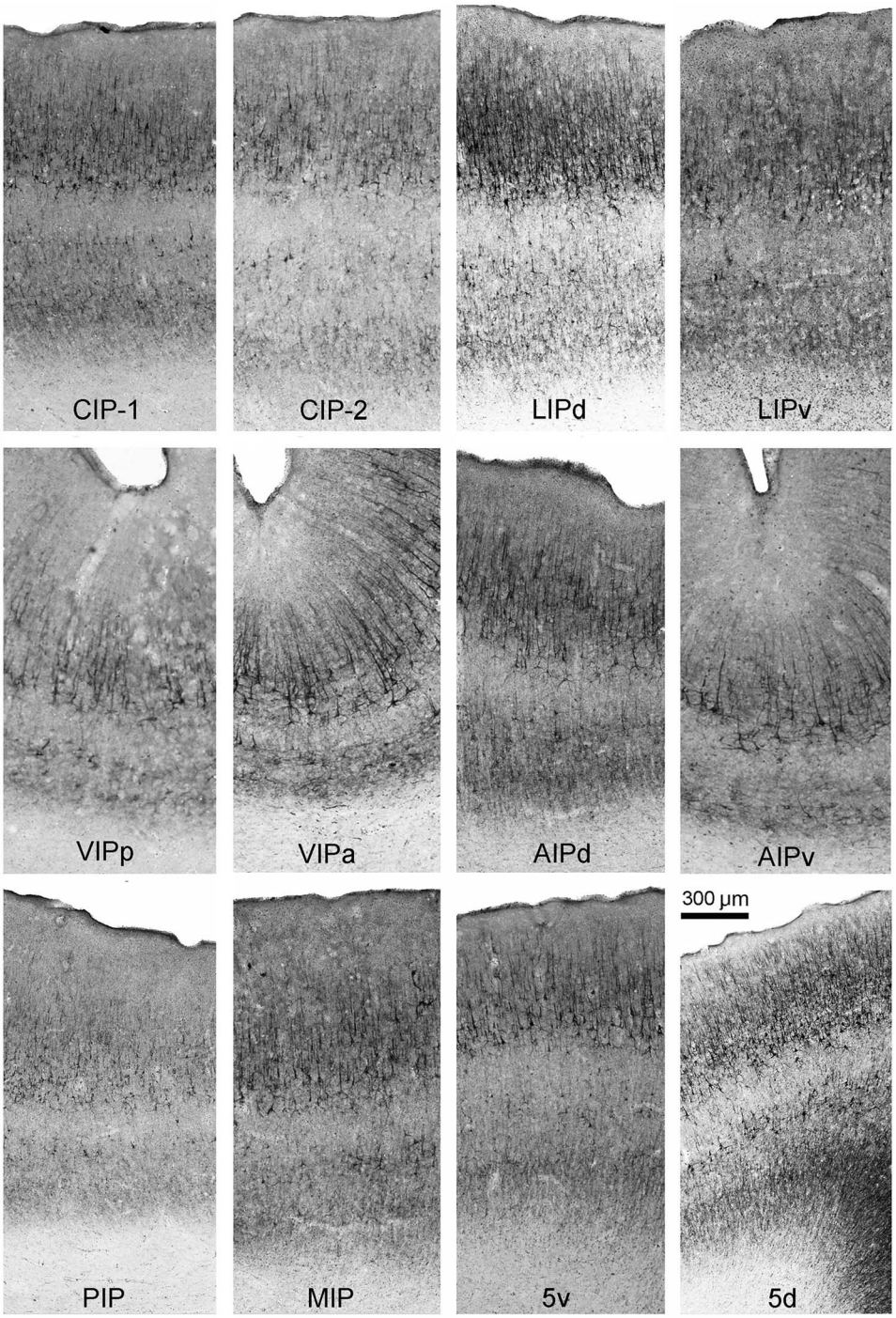

FIGURE 4 High power photomicrographs of the IPS areas revealed by SMI-32 immunohistochemistry shown in Figure 3. See Results for a detailed description of the immunoarchitectural organization of each area. Small to large pyramidal neurons, including their proximal processes and fragments of apical dendrites, were the main structures revealed by SMI-32 immunostaining. Immunoreactivity was strongest in layers III and V, as evident by the two bands that can be observed with varying degrees of intensity in all panels

3.4 | LIPd

Area LIPd is located medially in the lateral bank of the IPS. It is limited dorsally by area 7, ventrally by LIPv, and anteriorly by AIPd. Area LIPd is characterized by moderate to intense immunoreactivity to SMI-32, especially in the supragranular layers, with a higher density of stained cells compared to neighboring areas AIPd and LIPv. Layer III contains large and midsize cell bodies with long apical dendrites. Area LIPd exhibits a very distinct immunoreactivity in the infragranular layers. Layer V is moderately to densely populated with small and midsize cell bodies and a dense neuropil, especially in the most medial portions of LIPd. Layer VI also contains a densely stained neuropil. Cat-301 immunohistochemistry allowed us to subdivide area LIPd in a posterior

J_ID: Customer A_ID: CNE24438 Cadmus Art: CNE24438 Ed. Ref. No.: CASA-JCN-17-0236.R1 Date: 4-April-18 Stage: Page: 12

(LIPdp) and an anterior (LIPda) portion. LIPdp is limited dorsally by 7a, ventrally by LIPvp, anteriorly by LIPda, and posteriorly by CIP-1. Area LIPdp is characterized by broad and dense Cat-301 labeling in layer III, and a strong labeling of scattered cell clusters in layer V and VI. The upper layers showed fine dense labeling of the neuropil. Area LIPda is limited dorsally by 7b, ventrally by LIPva, anteriorly by AIPdp and AIPda, and posteriorly by LIPdp. It is characterized by a less dense Cat-301 labeling in layers III and V as compared to LIPdp.

3.5 | LIPv

Area LIPv is located medially in the lateral bank of the IPS, ventral to LIPd. It is limited ventrally by VIP and anteriorly by AIPd. Area LIPv is characterized by low to moderate immunoreactivity to SMI-32, with a lower density of stained cells than neighboring areas LIPd and AIPd. Area LIPv presents midsize neurons with short dendrites in layer III and exhibits a very distinct light immunoreactivity in the infragranular layers. Layer V is sparsely populated by small and midsize cells. We found moderate immunostaining of the neuropil in layer V (especially in the most medial portion of LIPv) and layer VI. In sections stained for Cat-301, area LIPv could also be subdivided into posterior (LIPvp) and anterior (LIPva) portions. Area LIPvp is limited dorsally by LIPdp, ventrally by VIPp, anteriorly by LIPva, and posteriorly by CIP-2. It is characterized by a medium-intensity Cat-301 labeling in inferior layer III, and an intermediate labeling in layers V and VI. The upper layers have a weak to medium-intensity labeling of the neuropil. Area LIPva is bounded dorsally by LIPda, ventrally by VIPa, anteriorly by AIPd, and posteriorly by LIPvp. It is characterized by a less dense Cat-301 labeling in layers III and V as compared to LIPvp.

3.6 | VIP

Area VIP is located at the floor of the IPS. It is limited dorsolaterally by LIPv, anteriorly by AIPv, and medially by PIP and MIP. Area VIP is characterized by a weaker immunoreactivity to SMI-32 than neighboring areas LIPv and MIP. It can be subdivided in posterior (VIPp) and anterior (VIPa) portions, where VIPa presents a higher density of pyramidal cells with long and well stained apical dendrites in layer III. Layer V is sparsely populated by midsize cell bodies, and showed weak neuropil labeling, especially at the medial-most portion of VIP. Layer VI exhibited light staining of the neuropil. In sections stained for Cat-301, VIP is characterized by a medium-intensity labeling in layers III and V. The upper layers show a faint labeling of the neuropil.

3.7 | AIPd

Area AIPd is located in the anterior portion of the lateral bank of the IPS. It is bounded dorsally by area 7, ventrally by AIPv and posteriorly by LIP. Area AIPd is characterized by moderate immunoreactivity to SMI-32, exhibiting a higher density of stained cells than neighboring areas LIPv and VIPa. Area AIPd exhibits a very distinct immunoreactivity in the infragranular layers, with an intense neuropil labeling but a small number of labeled cells. AIPd is characterized by medium-intensity Cat-301 labeling in layer III. The upper layers show a fine light labeling of the neuropil. The connectivity data suggest a further subdivision of AIPd into AIPdp and AIPda.

3.8 | AIPv

Area AIPv is located anteriorly at the floor of the IPS. It is bounded dorsally by AIPd, medially by area 5v, and posteriorly by VIP. Area AIPv is characterized by low to moderate immunoreactivity to SMI-32, with a lower density of labelled cells than in neighboring areas AIPd and 5v, but with a higher density of labeling than in areas LIPv and MIP. We found midsize cell bodies with apical projections in the supragranular layers. Layer V was sparsely populated by small and midsize cell bodies. Layer VI exhibited intense labeling of the neuropil. AIPv is characterized by medium-intensity, spatially restricted Cat-301 labeling in layer III, and a medium-intensity labeling in layer V. The upper layers show a weak light labeling of the neuropil.

3.9 | PIP

Area PIP is located in the medial (anterior) bank of the IPS. It is limited dorsally by area 5v, ventrally by VIPp, anteriorly by MIPv, and posteriorly by POd and DM. PIP exhibits a lighter SMI-32 staining than neighboring areas 5v, MIP, and VIP. It shows a small number of stained cells in layer III and IV, and practically no labeled cells in layer VI. In sections stained for Cat-301, we could subdivide PIP into ventral (PIPv) and dorsal (PIPd) portions, where PIPv presents a stronger labeling than PIPd. It shows strongly stained and tightly packed pyramidal and stellate neurons in layers III and V.

3.10 | MIP

Area MIP is located in the medial bank of the IPS. It is limited ventrally by VIPa, posteriorly by PIP and dorsoanteriorly by area 5v. It is characterized by an intermediate immunoreactivity to SMI-32. The staining of the supragranular layers is clearly lighter than in area 5v, but similar to area VIP. Furthermore, the supragranular layers of MIP were thicker than the ones found in neighboring areas, especially layers I and II, which showed lighter immunostaining. A small number of cell bodies were observed in the infragranular layer V. Layer VI showed weak labeling of the neuropil. In sections stained for Cat-301, area MIP can be subdivided into ventral (MIPv) and dorsal (MIPd) portions. The overall staining intensity in area MIPv is clearly weaker than in MIPv and area 5d. MIPd is characterized by a medium-density diffuse Cat-301 labeling in layer III, and intermediate labeling in layer V. The upper layers show a fine lightly labeled neuropil.

3.11 | Area 5

Area 5 is located in the medial lip of the IPS. Similar to the parietal lobe partitioning described for the macaque monkey (Lewis & Van Essen, 2000), area 5 in the capuchin monkey is subdivided into two anatomically different sectors, namely areas 5-dorsal (5d) and 5-ventral (5v). The immunoarchitecture of area 5d based SMI-32 immunohistochemistry was previously described by our group (Mayer et al., 2016).

3.12 | Area 5d

Area 5d is limited ventrally by area 5v, and posteriorly by MIPd. In sections stained for SMI-32, area 5d presents intense immunoreactivity. Both supragranular and infragranular layers are distinctly darker and

J_ID: Customer A_ID: CNE24438 Cadmus Art: CNE24438 Ed. Ref. No.: CASA-JCN-17-0236.R1 Date: 4-April-18 Stage: Page: 13

thicker than in neighboring areas 5v and 2. Layer III contains a dense population of cell bodies with short apical projections. Label V contains a moderate to dense population of cell bodies. Layer VI exhibits a very intense labeling of the neuropil. Area 5d is characterized by strong Cat-301 labeling in layer III, and a small number of labeled cells in layer V. The upper layers have a fine to medium intensity labeling of the neuropil.

3.13 | Area 5v

Area 5v is limited dorsally by area 5d and ventrally by AIPv and MIPd. In SMI-32 reacted sections, area 5v exhibits intermediate immunoreactivity (weaker than in area 5d), but the labeling is still stronger than the one found in MIP. Layer III of area 5v exhibits a low to moderate density of cell bodies containing long apical projections. Layer V contains a low density of cell bodies. Layer VI exhibits a weak to moderate staining of the neuropil. We find a medium intensity and spatially diffuse Cat-301 labeling in layer III, and an intermediate labeling in layer V. The upper layers have a faint light labeling of the neuropil.

3.14 | Areas PO (V6), POd (V6A), V3, V3A, DI, and DM

In oblique histological sections stained for Cat-301, we are able to differentiate the cortical areas located in the annectant gyrus, in the floor of the posterior IPS and in the anterior lunate sulcus. Area PO is located in the anterior wall of the PO cleft. It is limited dorsally by POd, ventrally and posteriorly by V2, and anteriorly by DM. It is characterized by medium-density Cat-301 labeling in layer III, and a low number of labeled cells in layer V. The upper layers show a weak light labeling of the neuropil. Area POd is limited anteriorly by PIP and is characterized by a low-density Cat-301 labeling, mostly restricted to layer III. Area DM is located more posteriorly in the annectant gyrus and is bounded by area V3. DM presents a more intense labeling than areas V3 and PO, with well stained neurons in layers III and V. Area DI, located anterior to V3, exhibits strong Cat-301 labeling, with a larger proportion of labeled cells in layer III, but also strong cell staining in layer V. V3A, located between DI and CIP-1, is clearly less densely stained than these neighboring areas.

3.15 | IPS projections to V4 and TEO

Complementary to the immunoarchitectural partitioning of the IPS based on Cat-301 and SMI-32 immunohistochemistry, we analyzed the spatial organization of the IPS projections in order to corroborate the areal borders established by the immunostaining. Specifically, we injected retrograde traces in areas V4, TEO, PO, and MT, and described the distribution of cell bodies in the IPS region. Figure 5 illustrates the injection sites in areas V4, TEO, PO, and MT (flat-mount preparations) in the six monkey cases studied. Due to the fact that we used different types of retrograde traces, we were able to inject more than one tracer type in different cortical regions of the same animal. We used electrophysiological recordings to estimate the compound representation (i.e., the aggregate receptive field) in the visual field of all the injection sites for a given tracer (Figure 5). Note that the tracer injections in V4 were restricted in their topographical location. Figure 6 illustrates the V4- and TEO-projection cells originating from the IPS for two representative cases studied. In general terms, most of the projections bounding to these two ventral-stream areas originate in the lateral bank and the posterior portion of the IPS. The ventral and dorsal portions of LIP, respectively, preferentially project to areas V4 and TEO. Both anterior and posterior regions of LIPv project to V4, while mostly the anterior region of LIPd projects to TEO. LIPdp does not show significant projections to either area, suggesting a partitioning of LIPd in its anteroposterior axis (consistent with the segregation revealed by Cat-301 immunostaining). We also observed a substantial amount of V4-projecting neurons originating from areas DM, PIP, DI, and CIP-1. Data from Case 1 (top row, left) and Case 2 (bottom row, left) are consistent with each other, but yielded different quantities of labeled neurons, because the Case 1 injection was comparatively smaller. Weak or no labeling was detected in the ventrocaudal portion of the IPS (i.e., area CIP-2) for both cases. Figure 6 (right column) displays the distribution of labeled neurons after injections of retrograde tracers in area TEO. The amount of tracer injected in Case 2 was less than in Case 1 (see Figure 5), thereby accounting for the different overall density of labeled neurons in the IPS. Apart from the high-density of labeled neurons in LIPda, TEO-projecting neurons were also found in LIPv and DM. We observed strong labeling of CIP-1, CIP-2, and DI in some but not all animals. VIP and most of the medial bank of the IPS showed no projections to either V4 or TEO.

In Figure 7 we split the projections originating from superficial versus deep layers of the IPS, while superimposing data from Cases 1–4. In general terms, we found a similar pattern of labeled neurons in superficial versus deep layers of the IPS that target areas V4 and TEO. For the V4-projecting neurons, in particular, we also found that the overall density of labeled cells in superficial and deep layers were quite similar (Figure 7, left column). However, there are some notable differences between the superficial versus deep layer projections. The projections from CIP-1 to V4 originated predominantly in the deep layers, as compared to the superficial ones. Additionally, the rather limited projections from LIPd to V4 also originated preferentially in the deep layers. Contrary to the V4-projecting neurons of the IPS, the TEO-projecting cells (Figure 7, right column) preferentially originate in the superficial layers, as compared to the deep ones. In addition, the projections originating in LIPv (posterior and anterior portions) that target TEO are found mainly in the superficial layers. Table 1 offers a detailed picture of the relative strength of the IPS projections, with data split for the six different studied cases, as well for the laminar profile (superficial vs. deep) of the labeled cell bodies. Table 2 conflates data for all cases but split for the laminar origin of the projections.

Figure 8 and Table 3 summarize the distribution of labeled cells in the IPS for the V4 and TEO injections. In Figure 8, labeled neurons from four cases and from all cortical layers are superimposed in order to reveal the entire extent of the IPS regions projecting to areas V4 and TEO. Despite some overlap, the combined results shown here confirm the ventral versus dorsal segregation of LIP projections targeting V4 and TEO, respectively. However, note that the posterior portion of

ID: jwaa3b2server Time: 10:45 I Path: //chenas03.cadmus.com/Cenpro/ApplicationFiles/Journals/Wiley/CNE#/Vol00000/180041/Comp/APPFile/JW-CNE#180041

J_ID: Customer A_ID: CNE24438 Cadmus Art: CNE24438 Ed. Ref. No.: CASA-JCN-17-0236.R1 Date: 4-April-18 Stage: Page: 14

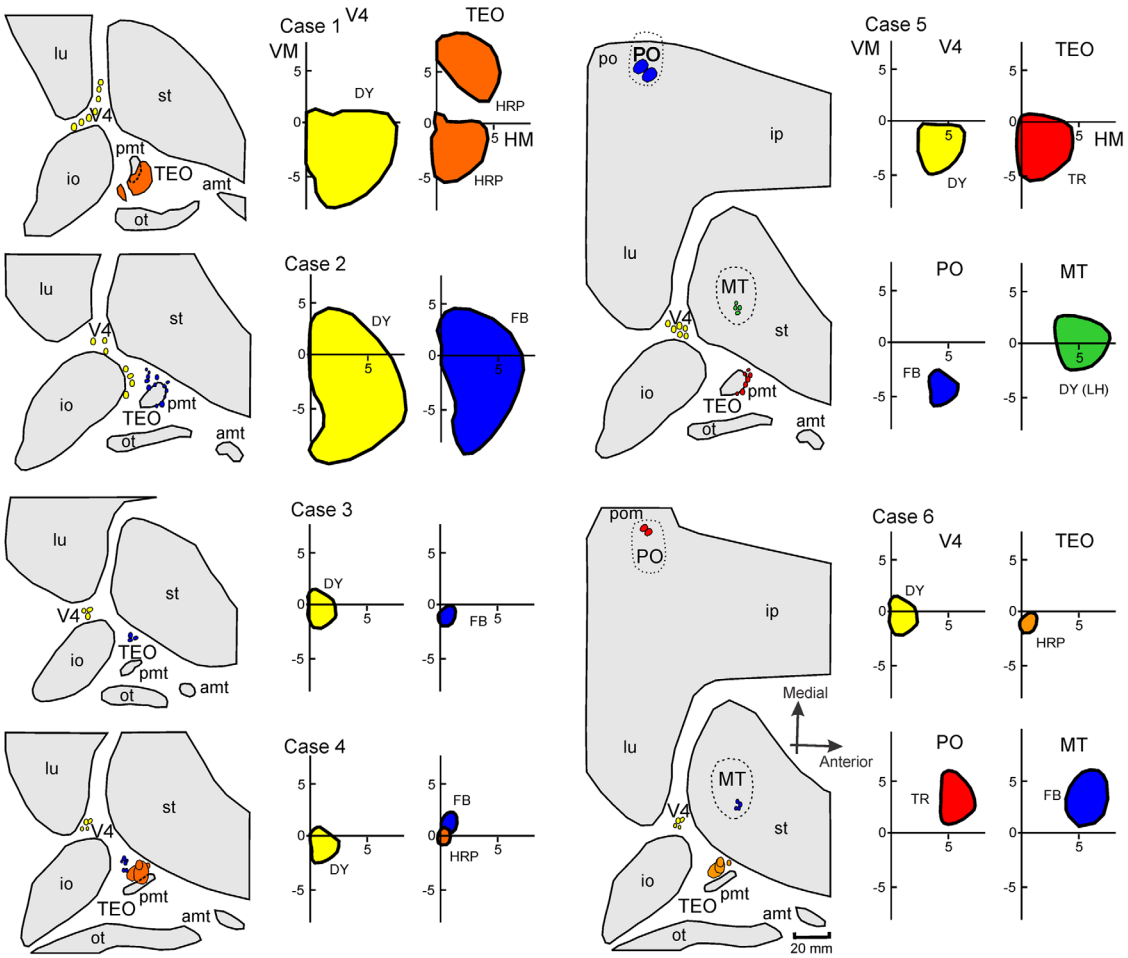

COLOR ONLINE AND BW IN PRINT

FIGURE 5 Retrograde tracer injection sites in areas V4, TEO, PO, and MT. The location and extent of the injection sites are depicted on flat-mount preparations of the cortex (posterior portion of the brain) for the six cases studied. Gray regions indicate cortical tissue normally buried inside sulci. Note that in most cases we made multiple, small injections that were placed within a limited region of the cortex, as indicated by the spheroid shapes of different colors. The visuotopic representation of the injection sites in the visual field is shown to the right of each corresponding flat-mount illustration. All injections (except the one in MT) were done in the right hemisphere. However, for visualization purposes, we plotted their visuotopy in a right-hemifield representation. The Cartesian coordinate system represents the visual field in degrees of visual angle, with the abscissa and the ordinate corresponding to the horizontal (HM) and vertical (VM) meridians, respectively. The type of tracer used for each injection is also indicated: DY, Diamidino Yellow; HRP, horseradish peroxidase; FB, fast blue and TR, Texas Red. Abbreviations: lu, lunate sulcus; io, inferior occipital sulcus; st, superior temporal sulcus; ot, occipito-temporal sulcus; po, parietal occipital sulcus; pmt, posterior medial temporal sulcus; amt, anterior medial temporal sulcus [Color figure can be viewed at wileyonlinelibrary.com]

LIPd projects to neither region. Additionally, CIP-2 projects to TEO, but not to V4. Finally, areas on the posterior portion of the IPS (DM, DI, and PIP) preferentially target V4 as compared to TEO.

3.16 | IPS projections to PO and MT

In addition to investigating the IPS projections to ventral-stream areas, such as V4 and TEO, we were also interested in describing the projection pattern from the IPS to areas belonging to the dorsal stream of visual information processing. We thereby injected retrograde tracers in areas MT and PO and evaluated the density of labeled cell bodies in the intraparietal areas. We selected these areas for two reasons. First, PO is a visual area located in the PO cleft, and therefore belongs to a region directly adjoining the IPS. Second, PO and MT belong to two distinct but complementary pathways of the dorsal stream, namely the dorsomedial and the dorsolateral sub-streams. Figure 9 illustrates the density of PO- and MT-projecting neurons originating in the superficial versus deep layers of the IPS for one case studied (Case 5; for results regarding the two cases analyzed see Tables 1–3). Notably, we observe robust neuronal projections originating in the medial bank and floor of the IPS to areas of the dorsal stream. These two IPS regions showed weak or absent projections to V4 and TEO. In general terms, PO-projecting neurons (Figure 9, left column) were found in similar densities in both superficial and deep cortical layers. The exceptions were PO-projecting neurons in AIPv, which were present only in the superficial layers, and PO-projecting neurons in AIPdp, which were present only in the deep layers. On the other hand, IPS neurons projecting to area MT originated preferentially in the deep cortical layers. Particularly, we found that the MT-projecting neurons originated only in the deep layers of VIP. In general, one of the strongest projections we

F9

J_ID: Customer A_ID: CNE24438 Cadmus Art: CNE24438 Ed. Ref. No.: CASA-JCN-17-0236.R1 Date: 4-April-18 Stage: Page: 15

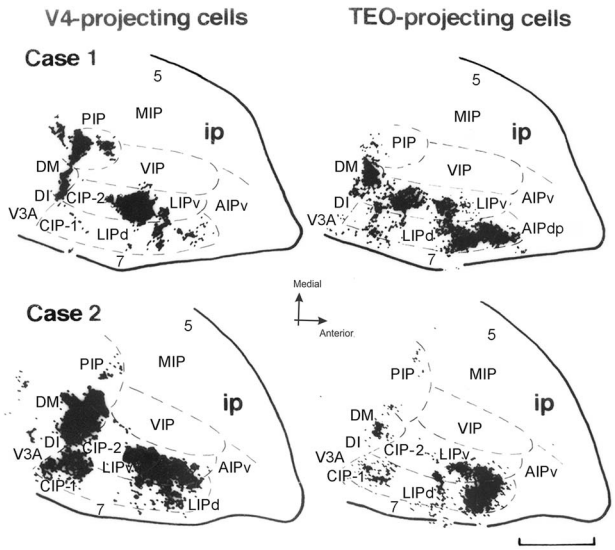

FIGURE 6 Distribution of V4- and TEO-projecting IPS neurons. Labeled cells, resulting from retrograde tracer injections in V4 and TEO (left and right columns, respectively), are plotted on histological sections of a flat-mount cortex cut parallel to the pial surface. Data for Cases 1 and 2 (top and bottom rows, respectively) are shown separately. Plots compile several superimposed sections. Dashed lines depict the estimated areal borders. Scale bar = 5 mm

found were the ones from MIP targeting PO. We found no projections from MIP to MT. Note that most of the IPS lateral bank projects to PO or MT in moderate to strong intensity. Projections originating in V3 and DM were also found.

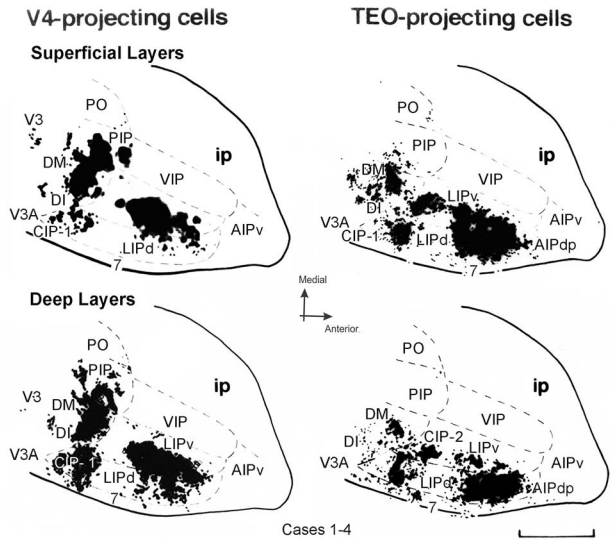

FIGURE 7 Differential distribution of V4- and TEO- projecting neurons across superficial versus deep cortical layers of the IPS. Here, we show a similar analysis to the one illustrated in Figure 6, but we now superimpose data from four different cases in order to reveal clusters of V4- or TEO- projecting neurons (left and right columns, respectively) originating from the superficial versus deep cortical layers (top and bottom rows, respectively) of the IPS. Dashed lines are the estimated areal borders. Scale bar = 5 mm

TABLE 2 Relative strength of the IPS projections to areas V4, TEO, PO, and MT

	V4		TEO		PO		MT	
	superf.	deep	superf.	deep	superf.	deep	superf.	deep
V3A	+	+	+	++	+			+
DI	++	+++	+	++	+		+	++
DM	+++	++	++	+	+	+	+	++
7a			+	+	+	+++		+
CIP-1	+	+++	++	++	+++	++	+	+
CIP-2			+++	+	+++	+		
LIPvp	+++	+++	+++	+	++	++	+	++
LIPva	++	+++	+++	+	+++	++	+	+
LIPdp			+	+	+	++	+	+
LIPda	++	+++	++++	+++	+	++	+	+
AIP v	+	+	+		++			
AIPdp	+					++	+	++
AIPda							+	+
VIPp	+	+			++	+++		++
VIPa					++	+++		++
PIP	+++	++	+		++++	+++		
MIP					++++	+++		
PO	+	+			n/a	n/a	+	++
5d	+					+	+	+

Same data as in Table 1, but conflated across cases and cortical layers. The label density assigned to each area was either the one attributed to the superficial or to the deep layer (see Table 1), whichever showed the highest value. The representation of label density follows the convention described in Table 1.

Figure 10 summarizes the IPS projections to areas V4, TEO, PO, and MT, split for their superficial versus deep laminar origin. Color intensity depicts connectivity strength (i.e., the average density of labeled neurons). Most of the projections arise from approximately 14 different IPS (CIP-1, CIP-2, PIP, VIPp, VIPa, MIP, LIPdp, LIPda, LIPvp, LIPva, AIPv,

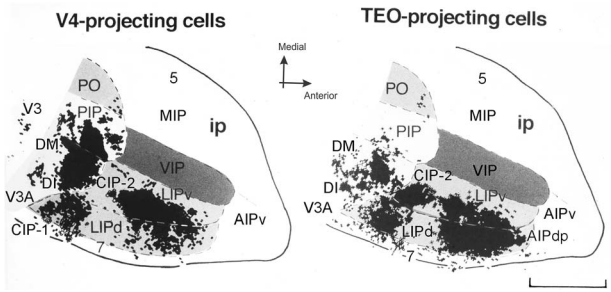

FIGURE 8 Overall distribution of V4- and TEO-projecting neurons across IPS areas. Here, we conflate data across cases and across cortical layers. The various IPS areas are highlighted in different shades of gray for visualization purpose. Scale bar = 5 mm

J_ID: Customer A_ID: CNE24438 Cadmus Art: CNE24438 Ed. Ref. No.: CASA-JCN-17-0236.R1 Date: 4-April-18 Stage: Page: 16

TABLE 3 Relative strength of the IPS projections to areas V4, TEO, PO, and MT

	V4	TEO	PO	MT
V3A	+	++	+	+
DI	+++	++	+	++
DM	+++	++	+	++
7a		+	+++	+
CIP-1	++	++	+++	+
CIP-2		+++	+++	
LIPvp	+++	+++	++	++
LIPva	+++	+++	+++	+
LIPdp		+	++	+
LIPda	+++	++++	++	+
AIP v	+	+	++	
AIPdp	+		++	++
AIPda				+
VIPp	+		+++	++
VIPa	+		+++	++
PIP	+++	+	++++	
MIP			++++	
PO	+		n/a	++
5d	+		+	+

Same data as in Table 1, but conflated across cases. The label density attributed to each area and cortical layer consists in the average labeling strength across cases (rounded to nearest integer, see Table 1). The representation of label density follows the convention described in Table 1.

AIPdp, AIPda, and 7a) and adjoining (DM, V3A, DI, PO, and POd) regions. The entire lateral bank projects to both ventral and dorsal streams. On the other hand, VIP (which is located at the floor of the IPS) and regions on the medial bank of the IPS (such as MIP) project predominately to dorsal stream areas and show weak or no projections to V4 and TEO. We observe that the IPS projections to the dorsal stream can be further segregated based on those targeting the dorsolateral (i.e., MT) versus the dorsomedial (i.e., PO) subdivisions. For example, MIP and AIPv project to PO but not MT. The anterior extent to which we found MT-projecting neurons at the floor of the IPS enabled us to define the border between VIP (which projects strongly to MT) and AIPv (which does not project to MT, as shown in Rosa, Soares, Fiorani, & Gattass, 1993). F10

4 | DISCUSSION

By combining immunoarchitectural and connectivity analysis, we were able to reliably partition the IPS into approximately 13 different cortical areas (CIP-1, CIP-2, PIP, VIPp, VIPa, MIP, LIPdp, LIPda, LIPvp, LIPva, AIPv, AIPdp, and AIPda). In addition to determining the borders of the classic intraparietal areas, some of which have been intensely studied using electrophysiological techniques and other approaches, we were able to further partition some of these regions into two or more subdivisions (e.g., LIPd and LIPv were each subdivided into anterior and posterior portions). Our proposed partitioning of the IPS offers an anatomical framework in which to guide future functional studies, and thereby advance us to a more complete understanding of the role of the different IPS areas in perception, action, and cognition.

4.1 | General organization of the IPS in New and Old World monkeys

Our work was performed in the capuchin monkey, a diurnal, midsized New World primate, comparable to the Old World monkey, *Macaca fascicularis*, in terms of brain size and sulcal pattern (Le Gros Clark, 1959; Freese & Oppenheimer, 1981). Additionally, previous work from our laboratory have shown extensive similarities in brain organization between the capuchin and Old World monkeys, such as the *M. fascicularis* and *M. mulatta* (Gattass et al., 2005). For example, our current results in the capuchin monkey IPS are consistent with those published by Colby et al. (1988), which studied the IPS of the *M. fascicularis*. Therefore, the organization of the IPS we describe here should be akin to the one found in Old World monkeys in general. The IPS of the capuchin is slightly more vertically orientated in the brain surface than the IPS in Old World monkeys. However, this divergence is small and does not impact the anatomical description we provide in Results regarding the relative disposition of the areas within the IPS.

Figure 11 summarizes our main conclusions. This summary figure is based on our previous work on Old World Monkeys (Colby et al., 1988; Gattass et al., 1997; Ungerleider et al., 2008) and on the present data. Although no one has yet carried out an electrophysiological mapping of CIP-1, CIP-2, VIP, MIP, PIP, or LIP, the connectional results suggest at least an upper versus lower field segregation of these areas. Note that the segregated clusters of labeled neurons in the IPS, following retrograde tracer injections in PO (Figure 11, top panel) allow us several conclusions. First, they indicate that areas CIP-1, CIP-2, LIP, VIP, PIP, and MIP all exhibit some degree of topographic organization. Areas PIP, MIP, and PCi represent a portion of the visual field that seems similar to the one represented by area PO, which emphasizes the visual periphery. VIP and LIP, in particular, are organized such that the superior and inferior hemifields are represented in their anterior and posterior portions, respectively. Second, areas CIP-1 and CIP-2 predominantly represent the superior visual hemifield. Third, labeled neurons in VIP, LIPv, and LIPd produce noncontiguous sets of clusters corresponding to the same PO injections. This result supports VIP as an independent area, as well as it supports the partitioning of LIP into ventral and dorsal portions. Fourth, projections to PO support V3d and V3v as a single and unique visual area. V3d is distinct from V2d, which contains an independent set of topographically organized labeled clusters. V3d is also distinct from V3A, which contains a representation of the upper and lower visual fields. Furthermore, immunoarchitectural data based on Cat-301 immunohistochemistry corroborate these conclusions. We planned the angle of histological sectioning to be oblique to the coronal plane. Therefore, we were able to capture within the same section the transition between regions in the IPS and those in the adjoining PO cleft/annectant gyrus. We observed two distinct areas, F11

ID: jwaa3b2server Time: 10:45 I Path: //chenas03.cadmus.com/Cenpro/ApplicationFiles/Journals/Wiley/CNE#/Vol00000/180041/Comp/APPFile/JW-CNE#180041

J_ID: Customer A_ID: CNE24438 Cadmus Art: CNE24438 Ed. Ref. No.: CASA-JCN-17-0236.R1 Date: 4-April-18 Stage: Page: 17

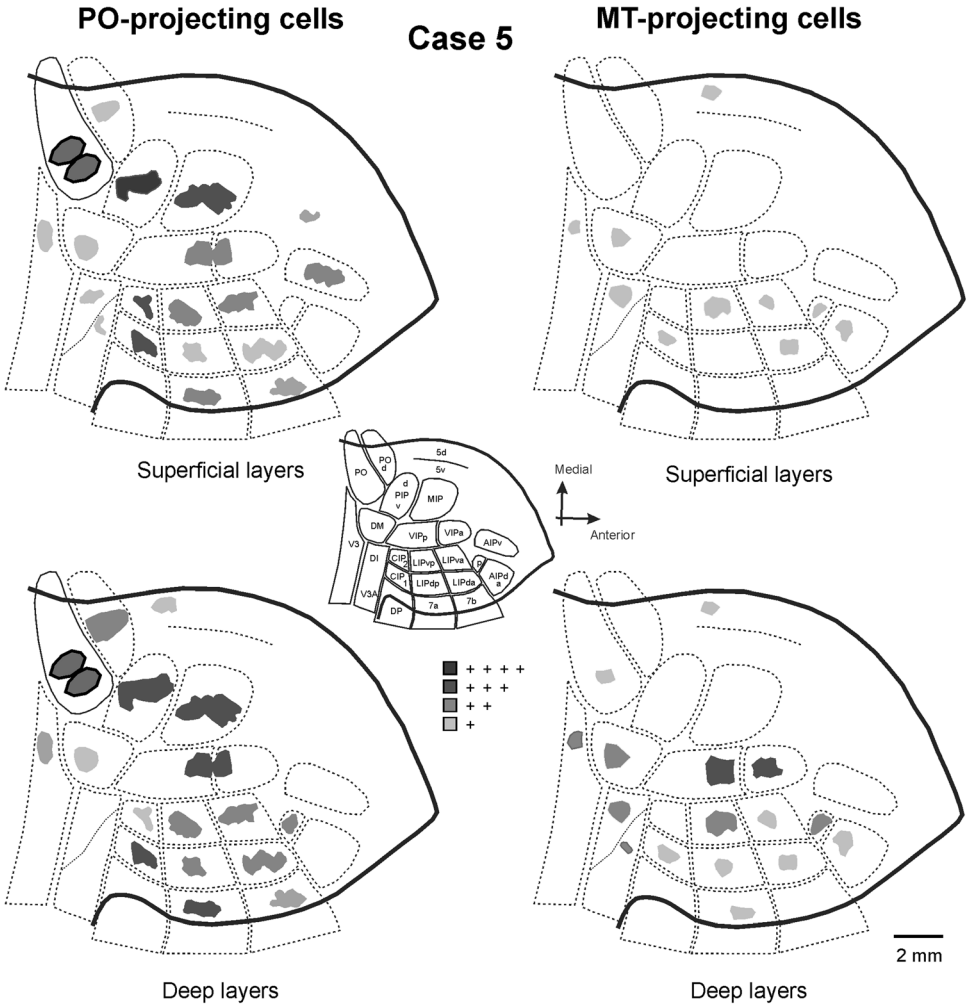

FIGURE 9 Differential distribution of MT and PO-projecting neurons across superficial versus deep cortical layers of the IPS. Two retrograde tracer injections, consisting of FB (area PO) and DY (area MT) were carried out in the right and left hemispheres, respectively, of the same individual (Case 5). For illustration purposes, both PO- and MT-projecting neurons are plotted on a right-hemisphere representation. The density of labeled neurons, where darker gray levels represent stronger labeling, are shown for the superficial (upper row) versus deep (lower row) cortical layers. Please refer to the center diagram for a correspondence between each IPS area and the dotted shapes depicted on the four surrounding plots. The two PO injection sites are indicated by the spheroids with continuous outlines. Area MT is not visible here

namely DM and DI, located anteriorly to V3d and medially to V3A. Finally, PO cannot be described as the portion of V3 that represents the peripheral visual field, since the PO injections produce an independent set of labeled clusters in V3d. Anterograde tracer injections in V2 also give rise to a cluster of labeled terminals in V3d, and another noncontiguous cluster in DM, lateral do PO. However, despite convincing immunoarchitectural data, we cannot fully discard the possibility that DM represents the peripheral visual field of V3d. Moreover, there is substantial variability between animals regarding the location, borders and extension of areas V3d, DM, V3A, DI, and PO. Future work will be required to clarify this issue.

Interestingly, anterograde tracer injections in area V2 alone are able to delimit VIP borders. This is supported by tracer injections in V4, which illustrate that PIP, VIP, and LIP receive projections predominately from the peripheral representation of the visual field (Figure 11, bottom right panel). Additionally, the injections show that the V2 projections reaching VIP are mainly those of the far-periphery representation of the visual field (see the spheroids and clusters with dashed outlines in Figure 11, bottom left panel). The arrangement of the labeled clusters corroborates the notion that the projections to the IPS areas have some degree of topographical organization. Within the IPS and adjoining regions, only PO, V3A, VIP, and LIP receive projections from V2, while PO, PIP, DI, V3A, DP, LIP, and VIP receive projections from V4. Results in Figure 11 also show that DI, V3A, DP, PIP, MIP, POd, CIP, LIP, VIP, and area 5d project to PO. Area POm at the medial surface of the hemisphere (as described by Rosa et al., 1993) also projects topographically to PO. Therefore, the differential projections to PO, V4, and V2 also confirm the segregation of the intraparietal areas described here.

4.2 | POm, PCi and the partitioning of V3, DM, V3A, and DI

We would like to propose two changes to our previously published reports (Colby et al., 1988; Gattass, Lima, Soares, & Ungerleider, 2015).

J_ID: Customer A_ID: CNE24438 Cadmus Art: CNE24438 Ed. Ref. No.: CASA-JCN-17-0236.R1 Date: 4-April-18 Stage: Page: 18

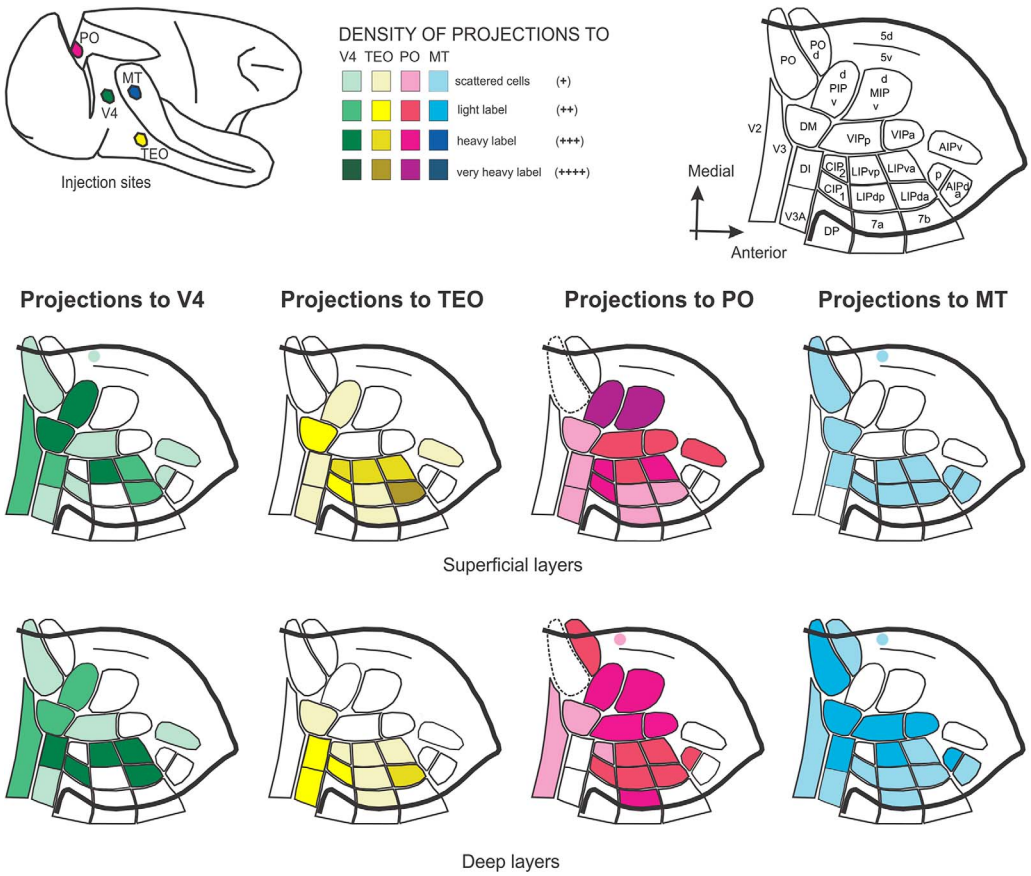

COLOR IN ONLINE AND PRINT

FIGURE 10 Summary of IPS partitioning based on its connectivity pattern and immunoarchitecture. Top left: location of the retrograde tracer injections. Top right: IPS partitioning based on the present work. The eight schemes below depict the density of labeled neurons across different IPS areas projecting to V4, TEO, PO, and MT (left to right columns, respectively). Data are shown separately for superficial versus deep cortical layers (top and bottom rows, respectively). Label density is assigned to one of five intensity levels, where darker shades correspond to no projection, scattered cells, light, heavy, and very heavy labeling, respectively). Results for each tracer were evaluated independently before merging the data

First, we would like to suggest a change in nomenclature for two cortical areas located medial to the IPS. In Colby et al. (1988), we designated POm as the area posterior to the cingulate sulcus. We would now like to re-designate this region as the parieto-cingulate area (PCi), due to its proximity to the cingulate sulcus (Figure 11, top panel). We now call the area immediately medial to PO and POd, and close to the medial branch of the PO cleft (i.e., the parieto-occipital medial sulcus or POmS), as the parieto-occipital medial area (POm). This change conforms to another report we have published (Rosa et al., 1993), where it seemed appropriate to name this area as POm. Second, we would like to suggest a possible subdivision of area V3d in the capuchin monkey into lateral and medial portions. The lateral portion will remain with the V3d designation, while the medial part would be designated as area DM. Likewise, V3A would also be subdivided into lateral and medial portions. The lateral portion corresponds to what was originally named V3A, while the medial portion would be designated as DI (see dotted lines between V3d and DM, and between V3A and DI in Figure 11, top panel). Note that this partitioning allows V3d and DM to retain a representation of the lower visual field, as both areas share the same clusters of labeled neurons. Similarly, it also allows V3A and DI to retain representations of the lower and upper visual hemifield representations. Previous reports have long suggested the existence of areas DM and DI in primate visual cortex (Allman & Kaas, 1975). By injecting retrograde tracer in MT, we were able to distinguish isolated clusters of labeled neurons in regions matching the location of the areas DM and DI. In addition, Cat-301 immunohistochemistry now provides an anatomic marker for their existence in the capuchin monkey (see Figure 1, Part II).

4.3 | Features of the primate IPS areas based on the current and previous work

The IPS is organized in a way that more perceptual related areas are located posteriorly, areas related to eye movements and movement perception in the near extrapersonal space are located at the central portion of the sulcus, and areas related to sensory motor components are located more anteriorly. These latter areas are richly interconnected with the frontal lobe and thereby participate in executive control. Lewis and Van Essen (2000), using myelin staining and SMI-32 immunohistochemistry, were able to identify 13 areas (17 architectonic subdivisions) in the IPS and PO regions of the macaque. Despite the terminological differences, the arrangement they describe is broadly similar to the one

J_ID: Customer A_ID: **CNE24438** Cadmus Art: **CNE24438** Ed. Ref. No.: **CASA-JCN-17-0236.R1** Date: **4-April-18** Stage: Page: **19**

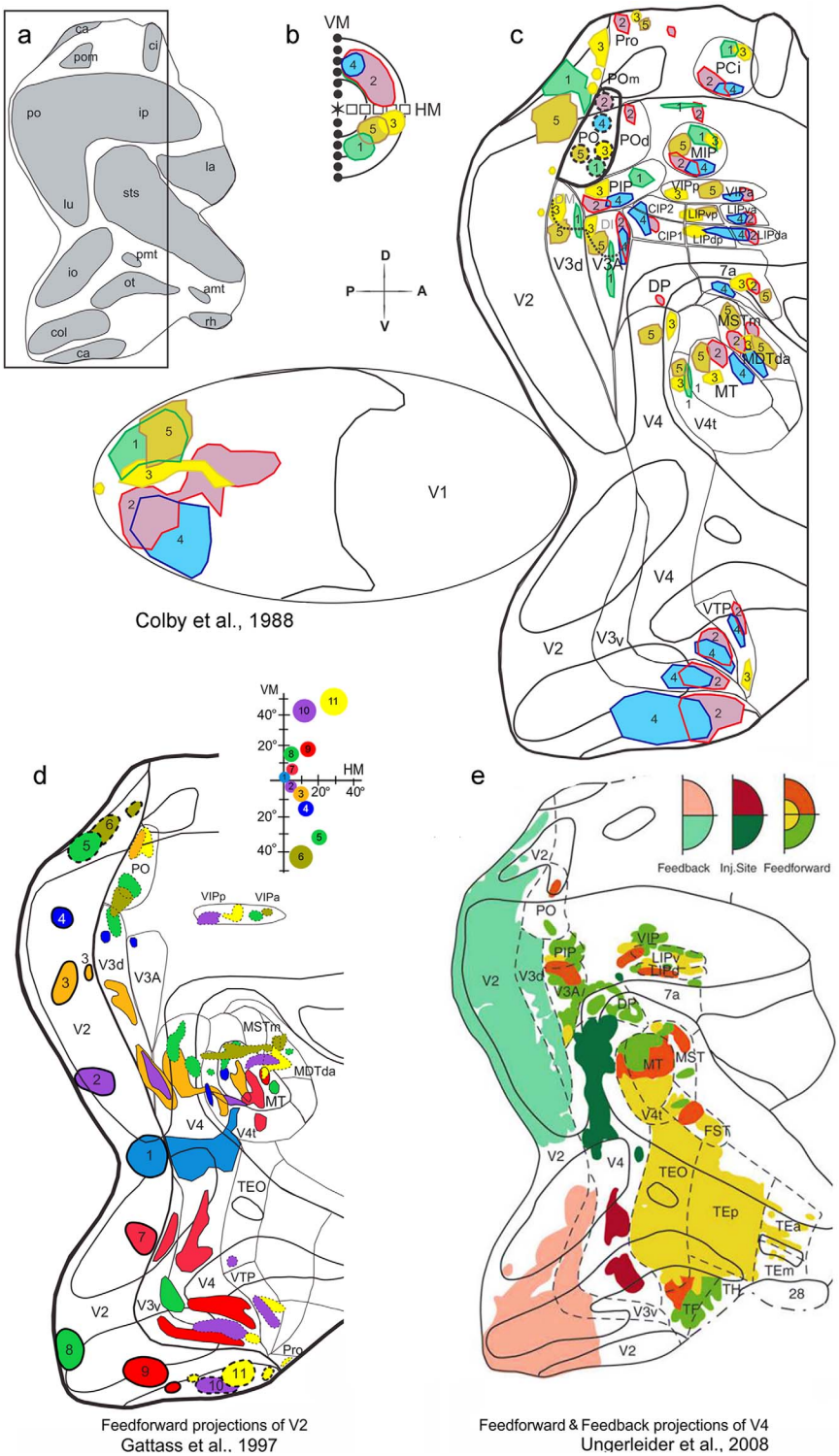

FIGURE 11 Flattened maps of the extrastriate cortex showing IPS partitioning based on its connectivity with areas V2, V4, and PO. Top panel: retrograde tracer injections in area PO (depicted by the dotted-lined colored circles numbered 1–5) reveal the pattern of projections from the IPS and surrounding regions to area PO (based on the present work, Colby et al., 1988; Gattass et al., 2015). Bottom left: anterograde tracer injections in V2 (depicted by the colored spheroids numbered 1–11) reveal the feedforward projections of V2 to several downstream visual areas (based on the work of Gattass et al., 1997). Injections carried out in the peripheral representation of V2 are indicated by the dotted outlines. The topographic representation of the V2 injections on the visual field are illustrated on the top of the panel. Of particular interest here are the V2 projections to PO and VIP. Bottom right: tracer injections in area V4 reveal that PIP, VIP, and LIP predominantly represent the peripheral visual field. The arrangement of the labeled clusters corroborates the notion that the projections to the IPS areas are topographically organized. The injection sites, as well as the labeled clusters of feedforward and feedback projections, are depicted in different colors and hues, as indicated on the top right portion of the panel (based on the work of Ungerleider et al., 2008). In all panels, clusters of labeled neurons follow the same color-coding as the one used for the injection site

J_ID: Customer A_ID: CNE24438 Cadmus Art: CNE24438 Ed. Ref. No.: CASA-JCN-17-0236.R1 Date: 4-April-18 Stage: Page: 20

of Preuss and Goldman-Rakic (1991), and of Pandya and collaborators (Seltzer & Pandya, 1980, 1986; Pandya & Seltzer, 1982). In most aspects, our IPS partitioning in the capuchin monkey resembles those described for the macaque. However, our IPS partitioning has revealed a comparatively higher number of areas. Below, we discuss the primate IPS areas based on the current and previous work.

4.4 | AIP

Area AIP was first described in the macaque monkey by Sakata et al. (1995) using electrophysiological criteria. It was characterized as a region located at the anterolateral portion of the IPS. Its neurons exhibited responses that were related to the visuomotor transformations for grasping. They also responded to object size, orientation and geometry (Murata et al., 2000). We found AIP to be subdivided into three subregions. We labeled the region anterior to VIP, located on the floor of the IPS, as AIPv. The adjoining region, lateral to AIPv, was labeled as AIPd, which we could further subdivide into anterior (AIPda) and posterior (AIPdp) portions, based on Cat-301 immunoarchitecture and connectivity. AIPda and AIPdp would jointly correspond to the AIP described by Sakata et al. (1995). What is the evidence that the region we designate as AIPv is not the anterior portion of VIP? MT is known to be strongly connected to VIP (Rosa et al., 1993; Ungerleider & Desimone, 1986a), but not with AIP (Borra et al., 2008). Here, we find MT-projecting neurons in the entire extent of VIP, but not on the region anterior to VIPa. Moreover, AIPv was found to be connected to PO. Connectivity data also allowed us to subdivide AIPd into posterior and anterior portions, since only the former showed projections to area PO. Finally, Cat-301 immunoarchitectural data corroborate the partitioning of the AIP into these three subregions, even though SMI-32 immunostaining was not able to distinguish AIPv from AIPd.

The AIP is known to be connected with the grasping-associated F5 pre-motor area (Borra et al., 2008). Clower, Dum, and Strick (2005), based on retrograde tracer injections in F5, defined the location of the capuchin monkey AIP as situated on the lateral outside lip of the IPS. We do not believe that the AIP defined by Clower et al., (2005) is equivalent to the one described here. The F5 projections they observe, in addition to targeting the lateral outside lip of the IPS, also project to the floor and lateral bank of the IPS, which is compatible with the AIP description offered here. Future electrophysiological work in the behaving monkey may be able to reveal if the neuronal response properties of AIPv is similar to the ones described by Sakata et al. (1995) for the AIP.

4.5 | CIP-1 and CIP-2

Arcaro, Pinsk, Li, and Kastner (2011) described two new visuotopically organized areas located in the caudolateral portion of the macaque monkey IPS, namely CIP-1 and CIP-2. We believe that the CIP-1 and CIP-2 areas we describe here in the capuchin monkey are equivalent to the ones reported by Arcaro et al. (2011). Previously, a rather homogeneous CIP area had been described in the region encompassing CIP-1 and CIP-2 (for review, see Van Essen, 2004). Cytoarchitectural, myeloarchitectural and connectivity criteria enabled us to distinguish CIP from the anteriorly located LIP area. Sakata (2003) showed that CIP neurons coded for the 3D shape of objects, thereby participating in visually guided grasping movements.

In our early work consisting of retrograde tracer injections in area MT (Rosa et al., 1993), we reported on a single MT-projection zone situated within the caudolateral IPS region that encompassed CIP and LIP. The reason we were not able to distinguish between CIP and LIP may have been because we used coronal sections of the IPS to analyze the density of labeled neurons. In the present work, we flattened the IPS cortex before plotting the labeled clusters, which might have increased the anatomical precision of our analysis. In subsequent work, using retrograde tracer injections in area PO (Colby et al., 1988), we report on clearly segregated clusters in caudolateral IPS, which would correspond to areas CIP and LIP. However, based on PO connectivity alone we were not able to distinguish between CIP-1 and CIP-2. In the current work, using a diverse set of retrograde tracer injections in areas MT, PO, TEO, and V4, we were capable of clearly segregating CIP-1 from CIP-2. In the ventrolateral IPS, TEO-projecting neurons originate from two noncontiguous clusters corresponding to CIP-2 and LIPv, respectively, which are located posteriorly and anteriorly. In dorsolateral IPS, TEO- and V4-projecting neurons also originate from two distinct clusters. Note that LIPdp, anterior to CIP-1, does not project to either V4 or TEO. Finally, Cat-301 and SMI-32 immunohistochemistry support the segregation of CIP-1 and CIP-2 based on neuronal architecture (compare the two panels on the top left of Figure 4). Both areas seem to preferentially represent the superior visual hemifield.

4.6 | LIP

LIP is part of a network of areas mediating saccadic eye movements. Additionally, its neurons are capable of fast remapping mechanisms that anticipate the future position of the eyes (Duhamel et al., 1992; Heide et al., 2001; Bisley & Goldberg, 2003a). These complex neuronal processes require the integration of visual and motor information. LIP receives input from several visual areas, and is interconnected with the frontal eye field (FEF) and the superior colliculus (Lynch, Graybiel, & Lobeck, 1985; Blatt, Andersen, & Stoner, 1990). Goldberg, Bisley, Powell, Gottlieb, and Kusunoki (2002) suggested that the activity of LIP neurons is not directly involved in generating saccades, but rather indicates the focus of attention (Bisley & Goldberg, 2003b). Projections from V4 (an area known to be involved in selective attention) to LIP are well established (Seltzer & Pandya, 1980; Rockland & Pandya, 1981; Andersen, Asanuma, Essick, & Siegel, 1990). Myeloarchitectural criteria are able to distinguish the ventral and dorsal portions of LIP. LIPv has a characteristic matted appearance, with fibers extending from layer VI all the way to the bottom of layer III (Rosa et al., 1993). Additionally, by comparing the results of retrograde tracer injections in V4 and TEO, we observe that ventral LIP preferentially projects to V4, while dorsal LIP preferentially projects to TEO (see Fig. 8). We have additionally partitioned the ventral and dorsal portions of LIP into anterior and posterior subdivisions based on connectivity and immunoarchitectural criteria. The topographic organization of PO-projecting

neurons indicate that the anterior and posterior portions represent, respectively, the superior and inferior visual hemifields (Colby et al., 1988; see Figure 11, top). LIPdp stood out as the one LIP subdivision that projected poorly or not at all to V4 or TEO.

4.7 | MIP and PIP

MIP and PIP are among least studied IPS areas. MIP is believed to participate in neural circuits involved in the planning, execution, and monitoring of reaching movements, and is thereby considered part of the parietal reaching region (Cohen & Andersen, 2002). MIP neurons are able to detect mismatches between reaching movements and target location (Desmurget & Grafton, 2000; Kalaska, Cisek, & Gosselin-Kessiby, 2003). Eskandar and Assad (1999) have shown that MIP neurons respond to the direction of hand movements toward a visual target. However, the impending correction mechanisms do not necessarily require a visual feedback of the moving hand, which indicates that they may rely on efference copy information, proprioceptive feedback and on an internal map of the target location (Kalaska et al., 2003).

Retrograde tracer injections in PO revealed several projection zones in the IPS (Colby et al., 1988). Based on the PO injections, the two PO-projecting zones that could be most clearly defined as unique IPS areas were PIP and MIP. This is because the five PO injections gave rise to five corresponding clusters of labeled neurons in each of these areas. Notably, both sets of clusters were well defined and topographically arranged, containing a representation of both lower and upper visual hemifields (see Figure 11, top). In the current work, we observe that MIP sends projections only to PO, and not to MT, V4, or TEO. These results indicate that MIP is part of the dorsomedial pathway of visual processing, which seems to remain segregated within the IPS. Based on Cat-301 immunostaining, we were able to clearly partition PIP and MIP into ventral and dorsal portions, which seem to correspond to the lower and upper visual hemifields representations, respectively. However, we did not observe any differential connectivity between ventral versus dorsal portions of PIP and MIP with areas V4, TEO, PO, and MT. Future studies will be required to address the functional distinction (if any) between MIPd versus MIPv, and between PIPd versus PIPv.

4.8 | VIP

VIP was first defined by Maunsell and Van Essen (1983) in the macaque monkey as one of the main feedforward targets of area MT to the IPS. Studies in other primate species have confirmed the interconnection between MT and areas of the ventral intraparietal cortex (Weller, Wall, & Kaas, 1984; Krubitzer & Kaas, 1990). Accordingly, stimuli conveying motion information have been demonstrated to activate VIP neurons (Colby et al., 1993; Bremmer, Duhamel, Ben Hamed, & Graf, 1997). Area VIP receives projections from motor, somatosensory, auditory and vestibular areas (Maunsell & Van Essen, 1983; Lewis & Van Essen, 2000), allowing its neurons to code space in head-centered coordinates for different stimulus modalities (Colby et al., 1993). Myeloarchitectonically, VIP is characterized as a lightly myelinated region at the bottom of the IPS in the macaque monkey (Colby et al., 1993). VIP in the capuchin monkey (Rosa et al., 1993) can be defined using the same architectonic criteria as in the macaque (Blatt et al., 1990). We were able to distinguish VIP from surrounding regions based on Cat-301 and SMI-32 immunostaining. VIP could also be segregated from laterally located LIP and CIP based on its preferential connectivity to the dorsal-stream areas PO and MT, as compared to the ventral-stream areas V4 and TEO. Finally, VIP could be sub-divided into anterior and posterior portions based on Cat-301 and SMI-32 immunoarchitecture (see Figures 2 and 4). The topographic organization of PO-projecting neurons in VIP (Colby et al., 1988) indicate that the superior and inferior hemifields are represented in the anterior and posterior portions of VIP, respectively. Apart from that, we obtained limited evidence based on connectivity data for an anterior versus posterior segregation of VIP. Future studies will be necessary to ascertain the functional differences between VIPa and VIPp.

4.9 | PO and POd

We were the first to define PO as a visual area located on the anterior bank of the PO cleft in the macaque monkey (Colby et al., 1988). A portion of PO is also situated on the ventral portion of the medial wall of the IPS. PO location in the capuchin monkey has been shown to be the same as in Old World monkeys. It exhibits a dense myelinated, matted pattern that stands out from the surrounding regions, similar to that found for area MT (Neuenschwander, Gattass, Sousa, & Piñon, 1994). Also, similar MT, PO receives direct feedforward projections from area V1 (Colby et al., 1988). However, electrophysiological mapping has shown that area PO emphasizes the representation of the peripheral visual field (Neuenschwander et al., 1994).

Dorsal to PO, we find area POd, which contains its own representation of the peripheral visual field, and which is not as densely myelinated as area PO (Neuenschwander et al., 1994). However, POd shows a denser myelination compared to the dorsally adjoining caudal subdivision of the somatosensory association cortex (area PE of Von Bonin & Bailey, 1947), or to the laterally adjoining area PIP (Neuenschwander et al, 1994). Area PO and POd have been defined as belonging to the dorsolateral pathway (Gattass et al., 1990; Nascimento-Silva et al., 2003), a subdivision of the dorsal pathway of visual information processing (Ungerleider & Mishkin, 1982). Our current results show that MIP projects to PO but not to MT, which belongs to the dorsolateral stream. These results suggest that PO and MIP may be part of a segregated visual pathway within the IPS (data unavailable for POd). However, of the four visual areas in which we carried out tracer injections (V4, TEO, PO, and MT), PO seemed to be area receiving the strongest projections from the IPS, suggestion a widespread integration of visual pathways within the IPS.

ACKNOWLEDGMENTS

We thank Edil Saturato da Silva Filho and Liliane H. Pontes for technical help. This work would not be possible without the aid of Maria Thereza A. Monteiro and Liliane H. Pontes in the preparation of the manuscript.

CONFLICT OF INTEREST

We declare that there is no conflict of interest, either financial, personal or other relationships with other people or organizations within three years of beginning the submitted work that could inappropriately influence the results or interpretation of the data of the manuscript.

AUTHOR CONTRIBUTIONS

All authors had full access to all the data in the study and take responsibility for the integrity of the data and the accuracy of the data analysis. Study concept and design: RG, OM. Acquisition of data: OM, RG, JGMS, AM. Analysis and interpretation of data: OM, RG, BL, JF, JGMS. Drafting of the manuscript: RG. Critical revision of the manuscript for important intellectual content: RG, BL, JMS, JF. Obtained funding: RG. Study supervision: RG.

ORCID

Bruss lima http://orcid.org/0000-0001-6865-2900
João G. Franca http://orcid.org/0000-0002-6774-5627
Ricardo Gattass http://orcid.org/0000-0002-0321-1490

REFERENCES

Allman, J. M., & Kaas, J. H. (1975). The dorsomedial cortical visual area: A third tier area in the occipital lobe of the owl monkey (Aotus trivirgatus). *Brain Research*, *100*, 473–487.

Andersen, R. A. (1989). Visual and eye movement functions of the posterior parietal cortex. *Annual Review of Neuroscience*, *12*, 377–403.

Andersen, R. A., Asanuma, C., Essick, G., & Siegel, R. M. (1990). Corticocortical connections of anatomically and physiologically defined subdivisions within the inferior parietal lobule. *Journal Comparative Neurology*, *296*, 65–113.

Arcaro, M. J., Pinsk, M. A., Li, X., & Kastner, S. (2011). Visuotopic organization of macaque posterior parietal cortex: A functional magnetic resonance imaging study. *The Journal of Neuroscience*, *31*, 2064–2078.

Bisley, J. W., & Goldberg, M. E. (2003a). The role of the parietal cortex in the neural processing of saccadic eye movements. *Advances in Neurology*, *93*, 141–157.

Bisley, J. W., & Goldberg, M. E. (2003b). Neuronal activity in the lateral intraparietal area and spatial attention. *Science (New York, N.Y.)*, *299*, 81–86.

Blatt, G. J., Andersen, R. A., & Stoner, G. R. (1990). Visual receptive field organization and cortico-cortical connections of the lateral intraparietal area (area LIP) in the macaque. *Journal Comparative Neurology*, *299*, 421–445.

Borra, E., Belmalih, A., Calzavara, R., Gerbella, M., Murata, A., Rozzi, S., & Luppino, G. (2008). Cortical connections of the macaque anterior intraparietal (AIP) area. *Cerebral Cortex*, *18*, 1094–1111.

Bremmer, F., Duhamel, J. R., Ben Hamed, S., & Graf, W. (1997). The representation of movement in near extra-personal space in the macaque ventral intraparietal area (VIP). In P. Thier, & H.O. Karnath (Eds), *Parietal lobe contributions to orientation in 3D space* (pp. 619–630). Heidelberg: Springer.

Campbell, M. J., & Morrison, J. H. (1989). Monoclonal antibody to neurofilament protein (SMI-32) labels a subpopulation of pyramidal neurons in the human and monkey neocortex. *Journal of Comparative Neurology*, *282*, 191–205.

Clower, D. M., Dum, R. P., & Strick, P. L. (2005). Basal ganglia and cerebellar inputs to 'AIP'. *Cerebral Cortex*, *15*, 913–920. DOI: https://doi.org/10.1093/cercor/bhh190.

Cohen, Y. E., & Andersen, R. A. (2002). A common reference frame for movement plans in the posterior parietal cortex. *Nature Review Neuroscience*, *3*, 553–562.

Colby, C. E., & Goldberg, M. E. (1999). Space and attention in parietal cortex. *Annual Review of Neuroscience*, *22*, 319–349.

Colby, C. L., & Duhamel, J. R. (1991). Heterogeneity of extrastriate visual areas and multiple parietal areas in the macaque monkey. *Neuropsychologia*, *29*, 517–537.

Colby, C. L., Duhamel, J. R., & Goldberg, M. E. (1993). Ventral intraparietal area of the macaque: Anatomic location and visual response properties. *Journal of Neurophysiology*, *69*, 902–914.

Colby, C. L., Gattass, R., Olson, C. R., & Gross, C. G. (1988). Topographical organization of cortical afferents to extrastriate area PO in the macaque: A dual tracer study. *Journal Comparative Neurology*, *269*, 392–413.

Cruz-Rizzolo, R. J., De Lima, M. A. X., Ervolino, E., de Oliveira, J. A., & Casatti, C. A. (2011). Cyto-, myelo- and chemoarchitecture of the prefrontal cortex of the Cebus monkey. *BMC Neuroscience*, *12*, 6.

Culham, J. C., & Kanwisher, N. G. (2001). Neuroimaging of cognitive functions in human parietal cortex. *Current Opinion in Neurobiology*, *11*, 157–163.

Desmurget, M., & Grafton, S. (2000). Forward modeling allows feedback control for fast reaching movements. *Trends of Cognitive Science*, *4*, 423–431.

DeYoe, E. A., Hockfield, S., Garren, H., & Van Essen, D. C. (1990). Antibody labeling of functional subdivisions in visual cortex: Cat-301 immunoreactivity in striate and extrastriate cortex of the macaque monkey. *Visual Neuroscience*, *5*, 67–81.

Duhamel, J. R., Colby, C. L., & Goldberg, M. E. (1992). The updating of the representation of visual space in parietal cortex by intended eye movements. *Science*, *255*, 90–92.

Eskandar, E. N., & Assad, J. A. (1999). Dissociation of visual, motor and predictive signals in parietal cortex during visual guidance. *Nature Neuroscience*, *2*, 88–93.

Freese, C. H., & Oppenheimer, J. R. (1981). The capuchin monkey, genus Cebus. In Coimbra-Filho A.F. & Mittermeier R.A. (Eds.) *Ecology and behavior of neotropical primates* (pp. 331–390). Rio de Janeiro: Academia Brasileira de Ciências.

Gallyas, F. (1979). Silver staining of myelin by means of physical development. *Neurological Research*, *1*, 203–209.

Gattass, R., Lima, B., Soares, J. G. M., & Ungerleider, L. G. (2015). Controversies about the visual areas located at the anterior border of area V2 in primates. *Visual Neuroscience*, *32*, E019.

Gattass, R., Nascimento-Silva, S., Soares, J. G., Lima, B., Jansen, A. K., Diogo, A. C., … Fiorani, M. (2005). Cortical visual areas in monkeys: Location, topography, connections, columns, plasticity and cortical dynamics. *Philosophical Transactions of the Royal Society, London - B Biological Science*, *360*, 709–731.

Gattass, R., Rosa, M. G. P., Sousa, A. P. B., Piñon, M. C. G., Fiorani, M., Jr., & Neuenschwander, S. (1990). Cortical streams of visual information processing in primates. *Brazilian Journal of Medical and Biological Research*, *23*, 375–393.

Gattass, R., Sousa, A. P., Mishkin, M., & Ungerleider, L. G. (1997). Cortical projections of area V2 in the macaque. *Cerebral Cortex (New York, N. Y. : 1991)*, *7*, 110–129.

Gattass, R., Sousa, A. P. B., & Gross, C. G. (1988). Visuotopic organization and extent of V3 and V4 of the macaque. *The Journal of Neuroscience*, *8*, 1831–1845.

Goldberg, M. E., Bisley, J., Powell, K. D., Gottlieb, J., & Kusunoki, M. (2002). The role of the lateral intraparietal area of the monkey in the generation of saccades and visuospatial attention. *Annals of the New York Academy of Science*, *956*, 205–215.

Gregoriou, G. G., Borra, E., Matelli, M., & Luppino, G. (2006). Architectonic organization of the inferior parietal convexity of the macaque monkey. *Journal Comparative Neurology*, *496*, 422–451.

Heide, W., Binkofski, F., Seitz, R. J., Posse, S., Nitschke, M. F., Freund, H. J., & Kömpf, D. (2001). Activation of frontoparietal cortices during memorized triple-step sequences of saccadic eye movements: An fMRI study. *European Journal of Neuroscience*, *13*, 1177–1189.

Hockfield, S., Mckay, R. D. G., Hendry, S. H. C., & Jones, E. G. (1983). A surface antigen that identifies ocular-dominance columns in the visual cortex and laminar features of the lateral geniculate nucleus. *Cold Spring Harbor Symposium on Quantitative Biology*, *48*, 877–889.

Hof, P. R., & Morrison, J. H. (1995). Neurofilament protein defines regional patterns of cortical organization in the macaque monkey visual system: A quantitative immunohistochemical analysis. *The Journal of Comparative Neurology*, *352*, 161–186.

Kalaska, J. F., Cisek, P., & Gosselin-Kessiby, N. (2003). Mechanisms of selection and guidance of reaching movements in the parietal lobe. *Advances in Neurology*, *93*, 97–119.

Krubitzer, L., & Kaas, J. H. (1990). Cortical connections of MT in four species of primates: Areal, modular, and retinotopic patterns. *Visual Neuroscience*, *5*, 165–204.

Le Gros Clark, W. E. (1959). *The antecedents of man*. Edinburgh: University Press.

Lewis, J. W., & Van Essen, D. C. (2000). Corticocortical connections of visual, sensorimotor, and multimodal processing areas in the parietal lobe of the macaque monkey. *Journal Comparative Neurology*, *428*, 112–137.

Luppino, G., Ben Hamed, S., Gamberini, M., Matelli, M., & Galletti, C. (2005). Occipital (V6) and parietal (V6A) areas in the anterior wall of the parieto-occipital sulcus of the macaque: A cytoarchitectonic study. *European Journal of Neuroscience*, *21*, 3056–3076.

Lynch, J. C., Graybiel, A. M., & Lobeck, L. J. (1985). The differential projection of two cytoarchitectonic subregions of the inferior parietal lobule of macaque upon the deep layers of the superior colliculus. *Journal Comparative Neurology*, *235*, 241–254.

Maunsell, J. H., & Van Essen, D. C. (1983). The connections of the middle temporal visual area (MT) and their relationship to a cortical hierarchy in the macaque monkey. *The Journal of Neuroscience*, *3*, 2563–2586.

Mayer, A., Nascimento-Silva, M. L., Keher, N. B., Bittencourt-Navarrete, R. E., Gattass, R., & Franca, J. G. (2016). Architectonic mapping of somatosensory areas involved in skilled forelimb movements and tool use. *Journal of Comparative Neurology*, *524*, 1399–1423. https://doi.org/10.1002/cne.23916.

McKay, R. D., & Hockfield, S. J. (1982). Monoclonal antibodies distinguish antigenically discrete neuronal types in the vertebrate central nervous system. *Proceedings of the National Academy of Sciences United States of America*, *79*, 6747–6751.

Mize, R. R., & Hockfield, S. (1989). Cat-301 antibody selectively labels neurons in the Y-innervated laminae of the cat superior colliculus. *Visual Neuroscience*, *3*, 433–443.

Murata, A., Gallese, V., Luppino, G., Kaseda, M., & Sakata, H. (2000). Selectivity for the shape, size, and orientation of objects for grasping in neurons of monkey parietal area AIP. *Journal of Neurophysiology*, *83*, 2580–2601.

Nascimento-Silva, S., Gattass, R., Fiorani, M., Jr., & Sousa, A. P. B. (2003). Three streams of visual information processing in V2 of Cebus monkey. *Journal Comparative Neurology*, *466*, 104–118.

Neuenschwander, S., Gattass, R., Sousa, A. P., & Piñon, M. C. (1994). Identification and visuotopic organization of areas PO and POd in Cebus monkey. *Journal Comparative Neurology*, *340*, 65–86.

Pandya, D. N., & Seltzer, B. (1982). Intrinsic connections and architectonics of posterior parietal cortex in the rhesus monkey. *Journal of Comparative Neurology*, *204*, 196–210.

Preuss, T. M., & Goldman-Rakic, P. S. (1991). Architectonics of the parietal and temporal association cortex in the strepsirhine primate Galago compared to the anthropoid primate Macaca. *The Journal of Comparative Neurology*, *310*, 475–506.

Rizzolatti, G., Luppino, G., & Matelli, M. (1998). The organization of the cortical motor system: New concepts. *Electroencephalography Clinical Neurophysiology*, *106*, 283–296.

Rockland, K. S., & Pandya, D. N. (1981). Cortical connections of the occipital lobe in the rhesus monkey: Interconnections between areas 17, 18, 19 and the superior temporal sulcus. *Brain Research*, *212*, 249–270.

Rosa, M. G., Soares, J. G., Fiorani, M., Jr., & Gattass, R. (1993). Cortical afferents of visual area MT in the Cebus monkey: Possible homologies between New and Old World monkeys. *Visual Neuroscience*, *10*, 827–855.

Rosa, M. G. P., Souza, A. P. B., & Gattass, R. (1988). Representation of the visual field in the second visual area in the *Cebus* monkey. *Journal of Comparative Neurology*, *275*, 326–345.

Sakata, H. (2003). The role of the parietal cortex in grasping. *Advances in Neurology*, *93*, 121–139.

Sakata, H., Taira, M., Murata, A., & Mine, S. (1995). Neural mechanisms of visual guidance of hand action in the parietal cortex of the monkey. *Cerebral Cortex*, *5*, 429–438.

Seltzer, B., & Pandya, D. N. (1980). Converging visual and somatic sensory cortical input to the intraparietal sulcus of the rhesus monkey. *Brain Research*, *192*, 339–351.

Seltzer, B., & Pandya, D. N. (1986). Posterior parietal projections to the intraparietal sulcus of the rhesus monkey. *Experimental Brain Research*, *62*, 459–469.

Soares, J. G., Rosado De Castro, P. H., Fiorani, M., Nascimento-Silva, S., & Gattass, R. (2008). Distribution of neurofilament proteins in the lateral geniculate nucleus, primary visual cortex, and area MT of adult *Cebus* monkeys. *The Journal of Comparative Neurology*, *508*, 605–614. https://doi.org/10.1002/cne.21718

Tsutsui, K., Jiang, M., Sakata, H., & Taira, M. (2003). Short-term memory and perceptual decision for three-dimensional visual features in the caudal intraparietal sulcus (Area CIP). *The Journal of Neuroscience*, *23*, 5486–5495.

Ungerleider, L. G., & Desimone, R. (1986a). Cortical connections of visual area MT in the macaque. *Journal of Comparative Neurology*, *248*, 190–222.

Ungerleider, L. G., & Desimone, R. (1986b). Projections to the superior temporal sulcus from the central and peripheral field representations of VI and V2. *Journal Comparative Neurology*, *248*, 147–163.

Ungerleider, L. G., & Mishkin, M. (1982). Two cortical visual svstems. In D.J. Ingle, M.A. Goodale, & R.J.W. Mansfield (Eds.) *Analysis of visual behavior* (pp. 549–586). Cambridge, MA: MIT Press.

Ungerleider, L. G., Galkin, T. W., Desimone, R., & Gattass, R. (2008). Cortical connections of area V4 in the macaque. *Cerebral Cortex (New York, N.Y. : 1991)*, *18*, 477–499.

Van Essen, D. C., Drury, H. A., Dickson, J., Harwell, J., Hanlon, D., & Anderson, C. H. (2001). An integrated software suite for surface-based analyses of cerebral cortex. *Journal of the American Medical Informatics Association*, *8*, 443–459.

Van Essen, D. C., & Maunsell, J. H. (1980). Two-dimensional maps of the cerebral cortex. *Journal of Comparative Neurology*, *191*, 255–281.

Van Essen, D. C. (2004). Towards a quantitative, probabilistic neuroanatomy of cerebral cortex. *Cortex*, *40*, 211–212.

Von Bonin, G., & Bailey, P. (1947). *The Neocortex of Macaca mulatta*. Urbana, IL: University of Illinois Press.

Webster, M. J., Bachevalier, J., & Ungerleider, L. G. (1994). Connections of inferior temporal areas TEO and TE with parietal and frontal cortex in macaque monkeys. *Cerebral Cortex*, *4*, 470–483.

Weller, R. E., Wall, J. T., & Kaas, J. H. (1984). Cortical connections of the middle temporal visual area (MT) and the superior temporal cortex in owl monkeys. *Journal of Comparative Neurology*, *228*, 81–104.

Zeki, S. M. (1978). The third visual complex of the rhesus monkey prestriate cortex. *Journal of Physiology*, *(London)*, *277*, 245–272.

How to cite this article: Mariani OS, Lima B, Soares JG, Mayer A, Franca JG, Gattass R. Partitioning of the primate intraparietal cortex based on connectivity pattern and immunohistochemistry for Cat-301 and SMI-32. *J Comp Neurol*. 2018;00:1–24. https://doi.org/10.1002/cne.24438

SGML and CITI Use Only
DO NOT PRINT

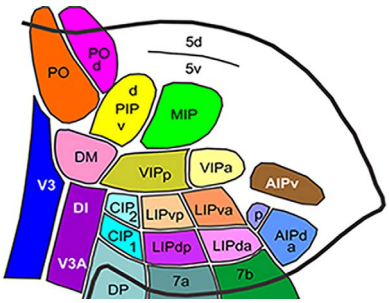

Visual areas of the intraparietal sulcus in the capuchin monkey. Two-dimensional reconstruction of the monkey cortex, showing the location of the extra-striate visual areas revealed by Cat-301 and SMI-32 immunohistochemistry. Most of these areas are differentially labeled after injections in V4, TEO, MT, and PO.